

Model adaptation in a discrete fracture network: existence of solutions and numerical strategies

Alessio Fumagalli¹

Francesco Saverio Patacchini²

¹ Department of Mathematics, Politecnico di Milano, p.za Leonardo da Vinci 32,
Milano 20133, Italy

² IFP Energies nouvelles, 1 et 4 avenue de Bois-Préau, 92852 Rueil-Malmaison, France

Abstract

Fractures are normally present in the underground and are, for some physical processes, of paramount importance. Their accurate description is fundamental to obtain reliable numerical outcomes useful, e.g., for energy management. Depending on the physical and geometrical properties of the fractures, fluid flow can behave differently, going from a slow Darcian regime to more complicated Brinkman or even Forchheimer regimes for high velocity. The main problem is to determine where in the fractures one regime is more adequate than others. In order to determine these low-speed and high-speed regions, this work proposes an adaptive strategy which is based on selecting the appropriate constitutive law linking velocity and pressure according to a threshold criterion on the magnitude of the fluid velocity itself. Both theoretical and numerical aspects are considered and investigated, showing the potentiality of the proposed approach. From the analytical viewpoint, we show existence of weak solutions to such model under reasonable hypotheses on the constitutive laws. To this end, we use a variational approach identifying solutions with minimizers of an underlying energy functional. From the numerical viewpoint, we propose a one-dimensional algorithm which tracks the interface between the low- and high-speed regions. By running numerical experiments using this algorithm, we illustrate some interesting behaviors of our adaptive model on a single fracture and small networks of intersecting fractures.

Keywords: *fractured porous media, adaptive constitutive law, variational formulation*

1 Introduction

Fractures are discontinuities, often assumed planar, along which a rock has been broken due to a pre-existing stress state, and represent the main conduits for fluid flow. Because of subsequent mineralization by chemical reactions along the fracture walls, a fracture may be partially or completely filled by material, substantially altering its physical properties and changing the fluid circulation. Additional rock deformation may change even more the hydraulic properties of the fractures. Even if there is not a clear separation of scales for fractures, since generally they span all sizes, we consider here only fractures at a certain scale leaving the smaller ones to be part of the rock matrix. A fracture's size has an impact on its aperture and consequently on its flow response.

Due to their geometrical complexity, fractures are normally represented as objects of co-dimension 1, meaning that in a d -dimensional porous medium they are approximated as $(d-1)$ -surfaces. This approach is normally referred to as discrete fracture model (DFM), see for

example [8, 9, 18, 20, 23, 24, 34, 41], where the physical processes involved are written as a set of partial differential equations with interface conditions between rock matrix and fractures. The resulting system is mixed-dimensional partial differential problem as discussed in [15, 16, 26, 29, 36]. For some specific problems the contribution of the rock matrix is negligible and can be omitted, obtaining the so-called discrete fracture network (DFN) models. On this topic, the reader may refer to [7, 10, 12, 13, 17, 21, 22, 28, 30] and the references therein. Especially in the presence of complex constitutive equations in the fractures, the authors in [1, 2] showed that it is possible to separate the contribution of the porous medium from the fracture network via a Robin-to-Neumann operator. They further showed that in a problem where fractures are modeled with a non-linear problem while the surrounding porous medium still obeys a linear law, it is possible to avoid the computationally expensive porous medium in the non-linear iterations considering only the fracture network. In the present work, we will consider only fracture networks while keeping in mind the possibility to include the surrounding porous medium via this approach.

Depending on several aspects, mainly the micro-structure and hydraulic aperture of a fracture, the flow in the fracture can be classified into different regimes corresponding to increasing flow rates and corresponding increasing mathematical and numerical difficulties. In many applications for low flow rates, caused by a combination of filling materials in the fracture and a relatively low-pressure gradient, Darcy flow can be considered in the fracture and a reduced model of Darcy-type can be derived, see among others [5, 20, 24–26, 34, 41], in the lower-dimensional setting. Most of the research so far has been focused on this flow model; however, its validity is questionable and, to a large extent, it is insufficient for real problems. For increased flow rates, for example when a fracture is an open and narrow channel or the packaging of grains is too coarse, viscous effects become important and a Brinkman or Stokes equation is more coherent as a reduced model to describe the flow; see [35, 39]. Finally for high velocities, because of inertial effects, experiments show deviations from the previous models, which indicate the need for a non-linear correction term. The authors in [27, 33] proposed a reduced model based on a Darcy–Forchheimer flow to capture this phenomenon. This effect is more evident in large objects like faults spanning several hundreds of meters. In all the lower-dimensional models, the flow in the surrounding rock matrix is still modeled by Darcy’s law and proper interface conditions are used to couple matrix and fracture flow.

Depending on their nature, fracture networks may exhibit all flow regimes in different regions separated by transition interfaces and coupled by suitable conditions. The interfaces can be located using Forchheimer and Reynolds numbers, see [43], which depend on the water velocity. This is the setting for the present paper, where the positions of the interfaces are not fixed at the outset of the problem: we obtain a (multi-physics) non-linear free-boundary problem on the fracture network. We present a mathematical framework that is able to adapt the constitutive law in accordance with the flow regime. As a simplification, we assume that only two laws, i.e., two speed regimes, can be prescribed, leaving the case of multiple laws as a future work. A theoretical analysis is developed along with a numerical algorithm that tracks the interface. Theoretically, we show existence of solutions to our problem via the minimization of an underlying energy. We do not show uniqueness since we make the choice to let the constitutive law linking velocity and pressure on the interface be a free parameter. We also show that the convex nature of the problem is strongly intertwined with the “direction” of the jump between the high-speed and low-speed laws; indeed, if the permeability increases from low- to high-speed the problem is non-convex, otherwise it is convex. In the former case

we are forced to restrict our existence result to one space dimension ($d = 1$). Numerically, the examples we give with one and more fractures illustrate the quality and applicability of the proposed algorithm, especially in the non-convex case. In the convex case, the algorithm often features oscillations between configurations which prevents it from converging. For the numerical simulations we used the library PorePy [32], a simulation tool written in Python for fractured and deformable porous media. PorePy is freely available on GitHub along with the numerical tests proposed in this work.

The paper is organized as follows. In Section 2 we describe our model, introduce the equations as well as some notation. In Section 3 we give the rigorous mathematical setting, along with the assumptions on the constitutive laws and the weak formulation of the problem. Section 4 is dedicated to our results on the existence of solutions and their proofs. Section 5 introduces the discrete formulation of the problem and a suitable algorithm to solve it. Numerical examples are reported in Section 6 for increasing geometrical and physical complexity. The work finishes with conclusions in Section 7.

2 Proposed model

We focus here on a single fracture; see Section 2.2 for a discussion on the model for multiple intersecting fractures. We identify our fracture with an open, bounded connected set $\Omega \subset \mathbb{R}^d$ with Lipschitz boundary $\partial\Omega$. We suppose Ω is filled with a fluid of constant density $\rho \equiv 1$. Mass conservation in Ω then reads

$$\operatorname{div} \mathbf{u} = q, \quad (1)$$

where $\mathbf{u}: \Omega \rightarrow \mathbb{R}^d$ is the unknown velocity of the fluid and $q: \Omega \rightarrow \mathbb{R}$ a given source term allowing, for instance, for fluid mass to be exchanged between the fractures and the surrounding porous medium, or rock matrix. Let $\Sigma_v, \Sigma_p \subset \partial\Omega$ be relatively open and such that $\partial\Omega = \overline{\Sigma_v \cup \Sigma_p}$ and $\Sigma_v \cap \Sigma_p = \emptyset$. To (1) we add the following boundary conditions:

$$\begin{cases} \mathbf{u} \cdot \mathbf{n} = u_0 & \text{on } \Sigma_v, \\ p = p_0 & \text{on } \Sigma_p, \end{cases} \quad (2)$$

where $p: \Omega \rightarrow \mathbb{R}$ is the unknown pressure of the fluid and \mathbf{n} is the outward normal unit vector of $\partial\Omega$. Here, $u_0: \Sigma_v \rightarrow \mathbb{R}$ and $p_0: \Sigma_p \rightarrow \mathbb{R}$ are given functions setting the conditions on the boundary on \mathbf{u} and p , respectively. We are denoting maps on Ω and their traces on the boundary $\partial\Omega$ by the same notation.

2.1 Velocity-pressure constitutive law

Typically, one couples (1) and (2) with a constitutive relation, or law, between the velocity field \mathbf{u} and the pressure field p via some operator Λ :

$$\Lambda(\mathbf{u}) = -\nabla p + \mathbf{f}, \quad (3)$$

where \mathbf{f} is a given body force (e.g., gravity). Examples of laws Λ relating velocity and pressure via (3) are

$$\begin{aligned} \Lambda_S(\mathbf{u}) &= -\Delta \mathbf{u}, & \Lambda_D(\mathbf{u}) &= \mathbf{K}^{-1} \mathbf{u}, \\ \Lambda_B(\mathbf{u}) &= -\Delta \mathbf{u} + \mathbf{K}^{-1} \mathbf{u}, & \Lambda_{DF}(\mathbf{u}) &= \mathbf{K}^{-1} \mathbf{u} + \alpha \|\mathbf{u}\|^{r-2} \mathbf{u}, \end{aligned} \quad (4)$$

where $\mathbf{K}: \Omega \rightarrow \mathbb{R}^{d \times d}$ is the permeability tensor and $\alpha \geq 0$ and $r \in [2, \infty)$ some parameters. The notation $\|\cdot\|$ stands for the Euclidean norm on \mathbb{R}^d . Choosing Λ_S gives Stokes' equation, Λ_D

gives Darcy’s equation, Λ_B gives Brinkman’s equation and Λ_{DF} gives the generalized Darcy–Forchheimer equation (which simplifies into the classical Darcy–Forchheimer when $r = 3$).

To the authors’ knowledge, a known issue that has not yet found a documented answer is the case when one needs to choose a combination of laws such as those given as examples in (4), rather than a single one, i.e., when one needs to couple different velocity–pressure laws according to some validity criterion which selects the better-adapted law. As already mentioned in the introduction, this criterion should depend on the speed regime (or Reynolds number) of the flow. For example, where the Reynolds number is low Darcy’s law Λ_D may be preferred, whereas where it is high the Darcy–Forchheimer law Λ_S might be chosen. For this reason, in this paper we consider the case where we need to choose from two laws Λ_1 and Λ_2 according to some threshold speed $\bar{u} > 0$. We expect that generalizing our results to more than two laws (for example having a low-speed regime, a transitional regime and a high-speed regime) should not be difficult. In this setting, the law operator in (3) takes the form

$$\Lambda(\mathbf{u}) = \begin{cases} \Lambda_1(\mathbf{u}) & \text{whenever } \|\mathbf{u}\| < \bar{u}, \\ \Lambda_2(\mathbf{u}) & \text{whenever } \|\mathbf{u}\| > \bar{u}. \end{cases} \quad (5)$$

Being able to impose a law at the interface $\{\|\mathbf{u}\| = \bar{u}\}$ is out of the scope of this paper—we will therefore consider our problem solved whenever we find a pressure field and a velocity field such that (1)–(3) and (5) hold. This summarizes as finding functions \mathbf{u} and p solving

$$\begin{cases} \operatorname{div} \mathbf{u} = q & \text{on } \Omega, \\ \Lambda(\mathbf{u}) = -\nabla p + \mathbf{f} & \text{on } \Omega, \\ \mathbf{u} \cdot \mathbf{n} = u_0 & \text{on } \Sigma_v, \\ p = p_0 & \text{on } \Sigma_p, \end{cases} \quad (6)$$

where Λ is any law such as in (5). Clearly, when $\Lambda_1 \neq \Lambda_2$, this choice of adaptable law introduces a discontinuity at $\|\mathbf{u}\| = \bar{u}$ which we shall treat carefully when studying existence of solutions. We will complete in Section 3.1 the strong formulation (6), which is somewhat formal since it lacks an interface constitutive relation; indeed, we will introduce a multi-valued weak setting so as to be able to treat the interface without imposing any given law on it. We refer the reader to [19] for a multi-valued monotone operator approach for pressure-dependent permeabilities; note that the operator therein is continuous in velocity.

Remark 2.1. *Whenever the boundary piece Σ_p is such that $\operatorname{Vol}^{d-1}(\Sigma_p) = 0$, where Vol^{d-1} stands for the $(d - 1)$ -dimensional Lebesgue measure, it is classical to add to (6) a constraint on the average of the pressure field:*

$$\frac{1}{|\Omega|} \int_{\Omega} p = \varpi, \quad (7)$$

for some $\varpi \in \mathbb{R}$. *Indeed, this is often required to ensure uniqueness of the pressure field satisfying Problem (6) when Λ is a classical continuous law. Similarly we will impose (7) whenever $\operatorname{Vol}^{d-1}(\Sigma_p) = 0$, so that our problem in this case becomes: find functions \mathbf{u} and p such that*

$$\begin{cases} \operatorname{div} \mathbf{u} = q & \text{on } \Omega, \\ \Lambda(\mathbf{u}) = -\nabla p + \mathbf{f} & \text{on } \Omega, \\ \mathbf{u} \cdot \mathbf{n} = u_0 & \text{on } \partial\Omega, \end{cases}$$

under the constraint (7), where $\mathbf{\Lambda}$ is now given in (5). For ease of discussion, however, we will often silence (7) and only refer to (6) as being our problem, even when $\text{Vol}^{d-1}(\Sigma_p) = 0$; this average condition will nevertheless be naturally encoded in our weak formulation.

We focus in this paper on Darcy-like operator laws, that is, laws involving no derivatives of the velocity field, so that we need to exclude Stokes' and Brinkman's equations as admissible examples. Under some additional conditions (depending in particular on the "direction" of the jump between laws $\mathbf{\Lambda}_1$ and $\mathbf{\Lambda}_2$ at the interface), we show existence of solutions via the study of an energetic formulation of (6). Indeed, we are able to define an energy functional on the space of velocity fields whose minimizers satisfy (6). Although we have uniqueness for this energetic formulation in some conditions (see Section 4), this property does not transfer to (6)—this is natural since we are not imposing what the velocity-pressure law should be on the interface. In order to hope for uniqueness, one should either impose an adequate law on the interface or show that the interface must have zero Lebesgue measure so that it does not play a role in defining weak solutions. As already mentioned, we do not wish to focus on the problem of the interface at this stage and leave it to a later work.

2.2 Intersecting fractures

In the case Ω is composed of multiple intersecting fracture branches, forming thus a fracture network, we can extend the previous model by including suitable conditions at the intersections. Given Ω we introduce $\omega^i \subset \Omega$ to be a fracture branch, with $n_\omega \ni i$ the total number of branches. Clearly, given two distinct branches ω^i and ω^j , with $i \neq j$, we have $\omega^i \cap \omega^j = \emptyset$ and also that $\bar{\Omega} = \bigcup_{i=1}^{n_\omega} \bar{\omega}^i$.

We consider $2 \leq n \leq n_\omega$ fracture branches that meet at an intersection \mathcal{I} whose closure $\bar{\mathcal{I}} = \bigcap_{i=1}^n \bar{\omega}^i$. To complete model (6) we impose the following conditions on \mathcal{I} :

$$\sum_{i=1}^n \mathbf{u}^i \cdot \mathbf{n}^i = 0 \quad \text{and} \quad p^i = p^j, \quad \forall i, j = 1, \dots, n, \quad (8)$$

where with a superscript i we indicate the corresponding object restricted to ω^i , and \mathbf{n}^i is a unit vector tangent to ω^i and pointing to \mathcal{I} , in the mono-dimensional case, and in addition normal to $\partial\omega^i$, in the multi-dimensional case. This condition is frequently used, see for instance [3, 4, 10, 11]. The first condition in (8) is a direct consequence of the conservation of mass at the intersection, while the second can be derived from each constitutive relation of the form (3). These conditions do not put any additional difficulties in the analysis and are therefore considered only in the numerical examples.

It is possible to consider more complex conditions that allow pressure and velocity jump at the intersection, see among others [8, 16, 25]. However, since this is not our main focus we keep the simpler interface condition (8).

3 Mathematical setting

We give in this section the rigorous mathematical setting; in particular we introduce the assumptions on the underlying law operators as well as the weak formulation of our problem. We shall use the convention to use boldfaced symbols for vectors and vector-valued functions.

From now on, without loss of generality we take \bar{u} to be equal to 1. For a given field $\mathbf{u}: \Omega \rightarrow \mathbb{R}^d$, we write

$$\begin{aligned}\Omega_1(\mathbf{u}) &= \{\mathbf{x} \in \Omega \mid \|\mathbf{u}(\mathbf{x})\| < 1\}, & \Omega_2(\mathbf{u}) &= \{\mathbf{x} \in \Omega \mid \|\mathbf{u}(\mathbf{x})\| > 1\}, \\ \Gamma(\mathbf{u}) &= \Omega \setminus (\Omega_1(\mathbf{u}) \cup \Omega_2(\mathbf{u})) = \{\mathbf{x} \in \Omega \mid \|\mathbf{u}(\mathbf{x})\| = 1\},\end{aligned}$$

where $\Omega_1(\mathbf{u})$, $\Omega_2(\mathbf{u})$ and $\Gamma(\mathbf{u})$ are what we have already respectively referred to as the *low-speed region*, *high-speed region* and *interface* (associated with \mathbf{u}). Obviously the family $\mathcal{C} := \{\Omega_1(\mathbf{u}), \Omega_2(\mathbf{u}), \Gamma(\mathbf{u})\}$ forms a partition of Ω , and we will refer to \mathcal{C} as the *configuration* of the problem, especially for the numerics in Sections 5 and 6. We can rewrite these sets in a more compact form:

$$\Omega_1(\mathbf{u}) = \mathbf{u}^{-1}(B_1(\mathbf{0})), \quad \Omega_2(\mathbf{u}) = \mathbf{u}^{-1}(E_1(\mathbf{0})), \quad \Gamma(\mathbf{u}) = \mathbf{u}^{-1}(S_1(\mathbf{0})),$$

where $B_1(\mathbf{0})$ and $S_1(\mathbf{0})$ stand respectively for the unit open ball and unit sphere in \mathbb{R}^d centered at the origin $\mathbf{0}$ and $E_1(\mathbf{0}) = \mathbb{R}^d \setminus (B_1(\mathbf{0}) \cup S_1(\mathbf{0}))$. Note that if \mathbf{u} is not continuous, then $\Omega_1(\mathbf{u})$ and $\Omega_2(\mathbf{u})$ may not be open.

For all $n \in [1, \infty)$, $m \in (0, \infty)$ and $A \subset \mathbb{R}^d$ measurable we will denote by $L^n(A)$ and $W^{m,n}(A)$ the Lebesgue space of measurable functions on A with integrable n th power and the m th-order Sobolev space associated to $L^n(A)$; we will also write $\mathbf{L}^n(A)$ in place of $(L^n(A))^d$. As usual, in these spaces, equality between two functions is always intended in the almost-everywhere sense.

3.1 Assumptions on the velocity-pressure laws

In the following, the operator laws $\mathbf{\Lambda}_1$ and $\mathbf{\Lambda}_2$ are assumed to be of the form

$$\mathbf{\Lambda}_1(\mathbf{u}) = \phi_1(\|\mathbf{u}\|^2)\mathbf{u} \chi_{\Omega_1(\mathbf{u})} \quad \text{and} \quad \mathbf{\Lambda}_2(\mathbf{u}) = \phi_2(\|\mathbf{u}\|^2)\mathbf{u} \chi_{\Omega_2(\mathbf{u})}, \quad (9)$$

where χ_A is the characteristic function of any set $A \subset \mathbb{R}^d$. The functions $\phi_1, \phi_2: [0, \infty) \rightarrow [0, \infty)$ are continuous and increasing on $[0, 1]$ and $[1, \infty)$, respectively. Furthermore, ϕ_2 satisfies the following assumption: there exist $r \geq 2$ and $c, C > 0$ such that

$$ca^{\frac{r-2}{2}} \leq \phi_2(a) \leq C \left(1 + a^{\frac{r-2}{2}}\right) \quad \text{for all } a \geq 1. \quad (10)$$

A recurrent notation we will use is

$$\lambda_1 := \phi_1(1) \quad \text{and} \quad \lambda_2 := \phi_2(1),$$

and will call the difference $\lambda_2 - \lambda_1$ the *interface inverse permeability jump*. Symmetrically, whenever $k_1 := 1/\lambda_1$ and $k_2 := 1/\lambda_2$ are considered (cf. in particular Sections 5 and 6), the difference $k_2 - k_1$ will be called the *interface permeability jump*. We will see that the sign of this jump is an important threshold which determines the convexity of the energy functional underlying the problem. Note that because ϕ_2 is increasing on $[1, \infty)$, one must have $c \leq \lambda_2$ and $C \geq \lambda_2/2$ in (10).

Interesting examples that fall into the above requests, in particular satisfying (9) with (10), are combinations of scalar versions of the Darcy and Darcy–Forchheimer laws $\mathbf{\Lambda}_D$ and $\mathbf{\Lambda}_{DF}$ (cf. (4)), as desired in the first place. Indeed, one is allowed to consider

$$\mathbf{\Lambda}_1(\mathbf{u}) = \lambda_1 \mathbf{u} \chi_{\Omega_1(\mathbf{u})} \quad \text{and} \quad \mathbf{\Lambda}_2(\mathbf{u}) = \lambda_2 \mathbf{u} \chi_{\Omega_2(\mathbf{u})},$$

that is, $\phi_1 \equiv \lambda_1$ and $\phi_2 \equiv \lambda_2$, or

$$\mathbf{\Lambda}_1(\mathbf{u}) = \lambda_1 \mathbf{u} \chi_{\Omega_1(\mathbf{u})} \quad \text{and} \quad \mathbf{\Lambda}_2(\mathbf{u}) = (\lambda_{21} + \lambda_{22} \|\mathbf{u}\|) \mathbf{u} \chi_{\Omega_2(\mathbf{u})}.$$

that is, $\phi_1 \equiv \lambda_1$ and $\phi_2(a) = \lambda_{21} + \lambda_{22} \sqrt{a}$, where λ_1 , λ_2 , λ_{21} and λ_{22} are positive scalars. In the former case we would require $r = 2$, whereas in the latter $r = 3$.

Remark 3.1. *This setting where $\mathbf{\Lambda}_1$ and $\mathbf{\Lambda}_2$ are as in (9) physically restricts us to scalar permeabilities. More general laws including tensor permeabilities, as motivated in [42], are for instance given by the following:*

$$\mathbf{\Lambda}_1(\mathbf{u}) = \phi_1(\boldsymbol{\lambda}_1 \mathbf{u} \cdot \mathbf{u}) \boldsymbol{\lambda}_1 \mathbf{u} \chi_{\Omega_1(\mathbf{u})}$$

and analogously for $\mathbf{\Lambda}_2$, where $\boldsymbol{\lambda}_1 \in \mathbb{R}^{d \times d}$ is a symmetric positive definite matrix encoding a tensor permeability. Even more general forms are envisageable:

$$\mathbf{\Lambda}_1(\mathbf{u}) = \sum_{j=1}^n \phi_{1,j}(\boldsymbol{\lambda}_{1,j} \mathbf{u} \cdot \mathbf{u}) \boldsymbol{\lambda}_{1,j} \mathbf{u} \chi_{\Omega_1(\mathbf{u})},$$

where the $\phi_{1,j}$ and $\boldsymbol{\lambda}_{1,j}$ are n different law functions and permeability tensors and the dot \cdot stands for the Euclidean inner product in \mathbb{R}^d . We leave these general laws to a future work. We claim that the techniques we use in the present paper for scalar laws should extend to tensor laws without too much difficulty.

We denote by $s = \frac{r}{r-1}$ the conjugate exponent of r . Thanks to the continuity of ϕ_1 and the right-hand inequality in (10), we observe that the operators $\mathbf{\Lambda}_1$ and $\mathbf{\Lambda}_2$ map $\mathbf{L}^r(\Omega)$ into $\mathbf{L}^s(\Omega)$. Because we allow for any law on the interface, this invites us to consider the multi-valued setting where our combined law $\mathbf{\Lambda}$ maps $\mathbf{L}^r(\Omega)$ into the power set $2^{\mathbf{L}^s(\Omega)}$ and is given by

$$\mathbf{\Lambda}(\mathbf{u}) = \begin{cases} \{\mathbf{\Lambda}_1(\mathbf{u})\} & \text{on } \Omega_1(\mathbf{u}), \\ \mathbf{L}^s(\Omega) & \text{on } \Gamma(\mathbf{u}), \\ \{\mathbf{\Lambda}_2(\mathbf{u})\} & \text{on } \Omega_2(\mathbf{u}), \end{cases}$$

which can equivalently be written as

$$\mathbf{\Lambda}(\mathbf{u}) = \{\mathbf{\Lambda}_1(\mathbf{u}) + \mathbf{\Lambda}_2(\mathbf{u}) + \mathbf{h} \chi_{\Gamma(\mathbf{u})}\}_{\mathbf{h} \in \mathbf{L}^s(\Omega)}. \quad (11)$$

Remark 3.2. *The existence results that we present in this paper still apply if we consider some “background” law with tensor permeability. Indeed, our proofs remain essentially untouched if the combined law $\mathbf{\Lambda}$ in (11) is replaced by*

$$\mathbf{\Lambda}(\mathbf{u}) = \{\beta(\boldsymbol{\lambda} \mathbf{u} \cdot \mathbf{u}) \boldsymbol{\lambda} \mathbf{u} + \mathbf{\Lambda}_1(\mathbf{u}) + \mathbf{\Lambda}_2(\mathbf{u}) + \mathbf{h} \chi_{\Gamma(\mathbf{u})}\}_{\mathbf{h} \in \mathbf{L}^s(\Omega)},$$

where $\boldsymbol{\lambda} \in \mathbb{R}^{d \times d}$ is symmetric positive definite and $\beta: [0, \infty) \rightarrow [0, \infty)$ is a continuous, increasing function such that $\beta + \phi_2$ satisfies (10) in place of ϕ_2 .

3.2 Weak formulation

We fix $q \in L^r(\Omega)$, $u_0 \in L^r(\Sigma_v)$, $p_0 \in W^{\frac{1}{r},s}(\Sigma_p)$ and $\mathbf{f} \in \mathbf{L}^s(\Omega)$. Consider the Sobolev space

$$\widetilde{W}^{1,s}(\Omega) = \begin{cases} \left\{ \xi \in W^{1,s}(\Omega) \mid \frac{1}{|\Omega|} \int_{\Omega} \xi = \varpi \right\} & \text{if } \text{Vol}^{d-1}(\Sigma_p) = 0, \\ \left\{ \xi \in W^{1,s}(\Omega) \mid \xi = p_0 \text{ on } \Sigma_p \right\} & \text{if } \text{Vol}^{d-1}(\Sigma_p) > 0, \end{cases}$$

where we recall that Vol^{d-1} is the $(d-1)$ -dimensional Lebesgue measure. The problem we shall focus on in the rest of the paper is: find $(\mathbf{u}, p) \in \mathbf{L}^r(\Omega) \times \widetilde{W}^{1,s}(\Omega)$ so that there exists $\mathbf{\Lambda}_u \in \mathbf{\Lambda}(\mathbf{u})$ such that for all $\varphi \in \mathbf{L}^r(\Omega)$ and $\psi \in \widetilde{W}^{1,s}(\Omega)$ there holds

$$\begin{aligned} \int_{\Omega} \mathbf{\Lambda}_u \cdot \varphi &= - \int_{\Omega} \nabla p \cdot \varphi + \int_{\Omega} \mathbf{f} \cdot \varphi, \\ \int_{\Omega} \nabla \psi \cdot \mathbf{u} &= - \int_{\Omega} q \psi + \int_{\Sigma_v} u_0 \psi, \end{aligned} \tag{12}$$

where we recall that $\mathbf{\Lambda}$ is given in (11). From the linearity of (12) with respect to the pressure field, we see that by setting $\mathbf{f}_0 = \mathbf{f} + \nabla(Ep_0)$, with $E: W^{\frac{1}{r},s}(\Sigma_p) \rightarrow W^{1,s}(\Omega)$ any extension operator being right-inverse of the $W^{1,s}(\Omega)$ -trace operator, and defining the Sobolev space

$$W_0^{1,s}(\Omega) = \begin{cases} \left\{ \xi \in W^{1,s}(\Omega) \mid \int_{\Omega} \xi = 0 \right\} & \text{if } \text{Vol}^{d-1}(\Sigma_p) = 0, \\ \left\{ \xi \in W^{1,s}(\Omega) \mid \xi = 0 \text{ on } \Sigma_p \right\} & \text{if } \text{Vol}^{d-1}(\Sigma_p) > 0, \end{cases}$$

the formulation in (12) is equivalent to: find $(\mathbf{u}, p) \in \mathbf{L}^r(\Omega) \times W_0^{1,s}(\Omega)$ so that there exists $\mathbf{\Lambda}_u \in \mathbf{\Lambda}(\mathbf{u})$ such that for all $\varphi \in \mathbf{L}^r(\Omega)$ and $\psi \in W_0^{1,s}(\Omega)$ there holds

$$\begin{aligned} \int_{\Omega} \mathbf{\Lambda}_u \cdot \varphi &= - \int_{\Omega} \nabla p \cdot \varphi + \int_{\Omega} \mathbf{f}_0 \cdot \varphi, \\ \int_{\Omega} \nabla \psi \cdot \mathbf{u} &= - \int_{\Omega} q \psi + \int_{\Sigma_v} u_0 \psi. \end{aligned} \tag{13}$$

We endow $W_0^{1,s}(\Omega)$ with the norm $\|\psi\|_{W_0^{1,s}(\Omega)} = \|\nabla \psi\|_{L^s(\Omega)}$ for all $\psi \in W_0^{1,s}(\Omega)$. We emphasize here that the well-posedness of (13) is not affected by the choice of the extension E in the definition of \mathbf{f}_0 .

Thanks to Riesz's representation theorem, we shall equivalently manipulate functions in $\mathbf{L}^s(\Omega)$ as elements of $(\mathbf{L}^r(\Omega))^*$, the dual of $\mathbf{L}^r(\Omega)$. In particular, this means that, given $\mathbf{u} \in \mathbf{L}^r(\Omega)$, operators $\mathbf{\Lambda}_u$ in $\mathbf{\Lambda}(\mathbf{u})$ will also be seen as maps from $\mathbf{L}^r(\Omega)$ to $(\mathbf{L}^r(\Omega))^* \sim \mathbf{L}^s(\Omega)$. Writing $\langle \cdot, \cdot \rangle$ the dual mapping on $\mathbf{L}^s(\Omega) \times \mathbf{L}^r(\Omega)$, the weak formulation in (13) of our problem can be restated as follows: find $(\mathbf{u}, p) \in \mathbf{L}^r(\Omega) \times W_0^{1,s}(\Omega)$ so that there exists $\mathbf{\Lambda}_u \in \mathbf{\Lambda}(\mathbf{u})$ such that for all $\varphi \in \mathbf{L}^r(\Omega)$ and $\psi \in W_0^{1,s}(\Omega)$ there holds

$$\begin{aligned} \langle \mathbf{\Lambda}_u, \varphi \rangle &= - \langle \nabla p, \varphi \rangle + \langle \mathbf{f}_0, \varphi \rangle, \\ \langle \nabla \psi, \mathbf{u} \rangle &= - \int_{\Omega} q \psi + \int_{\Sigma_v} u_0 \psi. \end{aligned} \tag{14}$$

Our goal is now to show existence for this weak formulation.

Remark 3.3. *We repeat here that, given the form of the law $\mathbf{\Lambda}$ in (9), we cannot get uniqueness of solutions—in fact of velocity fields—satisfying (14) since it is embedded in the very formulation of the problem that any interface velocity-pressure law is admissible. Uniqueness could be obtained if an appropriate interface law were imposed or if the interface were shown to be less than d -dimensional and therefore had no contribution in the definition of weak solutions.*

4 Existence

We state and prove here our results on existence for Problem (14). As already mentioned, we will see that our results depend on the sign of the interface inverse permeability jump, $\lambda_2 - \lambda_1$. The strategy is the following:

1. we reduce Problem (13) on the velocity and pressure fields into an equivalent problem on the velocity field only (cf. (16) and [6, 40]);
2. we derive an energetic formulation whose minimizers are solutions to this reduced problem on the velocity field (cf. (20) and [42]);
3. we study the existence of minimizers for this energetic formulation distinguishing the convex case $\lambda_1 \leq \lambda_2$ from the non-convex case $\lambda_1 > \lambda_2$ (cf. Theorems 4.7 and 4.8). We are only able to treat the one-dimensional setting $d = 1$ when $\lambda_1 > \lambda_2$.

4.1 Reduction to a problem on the velocity field

Define the maps $B: \mathbf{L}^r(\Omega) \rightarrow (W_0^{1,s}(\Omega))^*$ and $B^*: W_0^{1,s}(\Omega) \rightarrow (\mathbf{L}^r(\Omega))^*$ by

$$B(\boldsymbol{\varphi})(\psi) = B^*(\psi)(\boldsymbol{\varphi}) = \langle \nabla \psi, \boldsymbol{\varphi} \rangle \quad \text{for all } \boldsymbol{\varphi} \in \mathbf{L}^r(\Omega) \text{ and } \psi \in W_0^{1,s}(\Omega), \quad (15)$$

Let us introduce the set

$$V = \{\boldsymbol{\varphi} \in \mathbf{L}^r(\Omega) \mid \forall \psi \in W_0^{1,s}(\Omega), \langle \nabla \psi, \boldsymbol{\varphi} \rangle = 0\},$$

which satisfies $V = \text{Ker}(B)$. We write $V^\perp \subset \mathbf{L}^s(\Omega)$ the polar subspace of V , that is, $V^\perp = \{\mathbf{g} \in \mathbf{L}^s(\Omega) \mid \forall \boldsymbol{\varphi} \in V, \langle \mathbf{g}, \boldsymbol{\varphi} \rangle = 0\}$, and $\mathbf{L}^r(\Omega)/V \subset \mathbf{L}^r(\Omega)$ the quotient space of $\mathbf{L}^r(\Omega)$ by V .

The following three lemmas are inspired from their equivalents in [6].

Lemma 4.1. *The maps B and B^* in (15) are isomorphisms from $\mathbf{L}^r(\Omega)/V$ to $(W_0^{1,s}(\Omega))^*$ and from $W_0^{1,s}(\Omega)$ to V^\perp , respectively.*

Proof. By [6, Lemma 2.1], it suffices to show that there exists $\gamma > 0$ such that

$$\inf_{\substack{\psi \in W_0^{1,s}(\Omega) \\ \psi \neq 0}} \sup_{\substack{\boldsymbol{\varphi} \in \mathbf{L}^r(\Omega) \\ \boldsymbol{\varphi} \neq \mathbf{0}}} \frac{\langle \nabla \psi, \boldsymbol{\varphi} \rangle}{\|\psi\|_{W_0^{1,s}(\Omega)} \|\boldsymbol{\varphi}\|_{\mathbf{L}^r(\Omega)}} \geq \gamma.$$

To this end, let $\psi \in W_0^{1,s}(\Omega)$ with $\psi \neq 0$. Then, by identifying $\mathbf{L}^s(\Omega)$ with $(\mathbf{L}^r(\Omega))^*$ we get

$$\|\psi\|_{W_0^{1,s}(\Omega)} = \|\nabla \psi\|_{\mathbf{L}^s(\Omega)} = \sup_{\substack{\boldsymbol{\varphi} \in \mathbf{L}^r(\Omega) \\ \boldsymbol{\varphi} \neq \mathbf{0}}} \frac{\langle \nabla \psi, \boldsymbol{\varphi} \rangle}{\|\boldsymbol{\varphi}\|_{\mathbf{L}^r(\Omega)}},$$

so that

$$1 = \frac{\|\psi\|_{W_0^{1,s}(\Omega)}}{\|\psi\|_{W_0^{1,s}(\Omega)}} = \sup_{\substack{\varphi \in L^r(\Omega) \\ \varphi \neq 0}} \frac{\langle \nabla \psi, \varphi \rangle}{\|\psi\|_{W_0^{1,s}(\Omega)} \|\varphi\|_{L^r(\Omega)}}.$$

Taking above the infimum over all $\psi \in W_0^{1,s}(\Omega)$ with $\psi \neq 0$ ends the proof. \square

Now, via the following two lemmas, we simplify our weak formulation (14) into a problem restricted to V (cf. (16) below).

Lemma 4.2. *There exists a unique $\hat{\mathbf{u}} \in L^r(\Omega)/V$ such that*

$$\langle \nabla \psi, \hat{\mathbf{u}} \rangle = - \int_{\Omega} q\psi + \int_{\Sigma_v} u_0\psi \quad \text{for all } \psi \in W_0^{1,s}(\Omega).$$

Proof. For all $\psi \in W_0^{1,s}(\Omega)$, let

$$F(\psi) = - \int_{\Omega} q\psi + \int_{\Sigma_v} u_0\psi.$$

Since we are assuming that $q \in L^r(\Omega)$ and $u_0 \in L^r(\Sigma_v)$, the map F is a well-defined linear map from $W_0^{1,s}(\Omega)$ into \mathbb{R} , i.e., $F \in (W_0^{1,s}(\Omega))^*$. By Lemma 4.1, we thus know there exists a unique $\hat{\mathbf{u}} \in L^r(\Omega)/V$ such that

$$\langle \nabla \psi, \hat{\mathbf{u}} \rangle = B(\hat{\mathbf{u}})(\psi) = F(\psi) = - \int_{\Omega} q\psi + \int_{\Sigma_v} u_0\psi \quad \text{for all } \psi \in W_0^{1,s}(\Omega),$$

which is the desired result. \square

Lemma 4.3. *The weak formulation (14) is equivalent to the following problem: find $\mathbf{v} \in V$ such that there exists $\mathbf{\Lambda}_v \in \mathbf{\Lambda}(\mathbf{v} + \hat{\mathbf{u}})$ satisfying*

$$\langle \mathbf{\Lambda}_v, \varphi \rangle = \langle \mathbf{f}_0, \varphi \rangle \quad \text{for all } \varphi \in V, \tag{16}$$

where $\hat{\mathbf{u}}$ is given by Lemma 4.2.

Proof. We first suppose that (\mathbf{u}, p) is solution to Problem (14). Then we decompose \mathbf{u} as $\mathbf{u} = (\mathbf{u} - \hat{\mathbf{u}}) + \hat{\mathbf{u}} =: \mathbf{v} + \hat{\mathbf{u}}$. By (14), there exists $\mathbf{\Lambda}_v \in \mathbf{\Lambda}(\mathbf{u}) = \mathbf{\Lambda}(\mathbf{v} + \hat{\mathbf{u}})$ such that

$$\langle \mathbf{\Lambda}_v, \varphi \rangle = \langle \mathbf{f}_0, \varphi \rangle \quad \text{for all } \varphi \in V.$$

Furthermore, for all $\psi \in W_0^{1,s}(\Omega)$ we find $\langle \nabla \psi, \mathbf{v} \rangle = \langle \nabla \psi, \mathbf{u} \rangle - \langle \nabla \psi, \hat{\mathbf{u}} \rangle = 0$, so that $\mathbf{v} \in V$ and \mathbf{v} satisfies Problem (16).

Suppose now that $\mathbf{v} \in V$ satisfies Problem (16). Then, $\mathbf{\Lambda}_v - \mathbf{f}_0 \in V^\perp$. By Lemma 4.1 we know \mathbf{B}^* is an isomorphism from $W_0^{1,s}(\Omega)$ to V^\perp , so that there exists a unique $p \in W_0^{1,s}(\Omega)$ with

$$\langle \mathbf{\Lambda}_v - \mathbf{f}_0, \varphi \rangle = \mathbf{B}^*(-p)(\varphi) = - \langle \nabla p, \varphi \rangle \quad \text{for all } \varphi \in L^r(\Omega).$$

Furthermore, writing $\mathbf{u} = \mathbf{v} + \hat{\mathbf{u}}$ we get

$$\langle \nabla \psi, \mathbf{u} \rangle = \langle \nabla \psi, \mathbf{v} \rangle + \langle \nabla \psi, \hat{\mathbf{u}} \rangle = \langle \nabla \psi, \hat{\mathbf{u}} \rangle = - \int_{\Omega} q\psi + \int_{\Sigma_v} u_0\psi,$$

since $\mathbf{v} \in V$. We thus have that (\mathbf{u}, p) satisfies Problem (14), with p unique. \square

4.2 Energetic formulation

We first give the definition of Fréchet subdifferential and strong local minimizer in our setting:

Definition 4.4 (Fréchet subdifferential and strong local minimizer). *Let $\mathcal{F}: V \rightarrow \mathbb{R}$. For all $\mathbf{v} \in V$ we define the (Fréchet) subdifferential $\partial\mathcal{F}(\mathbf{v})$ of \mathcal{F} at \mathbf{v} by:*

$$\mathbf{g}_{\mathbf{v}} \in \partial\mathcal{F}(\mathbf{v}) \iff \mathbf{g}_{\mathbf{v}} \in V^* \text{ and } \forall \varphi \in V, \liminf_{\delta \rightarrow 0^+} \frac{\mathcal{F}(\mathbf{v} + \delta\varphi) - \mathcal{F}(\mathbf{v})}{\delta} \geq \langle \mathbf{g}_{\mathbf{v}}, \varphi \rangle.$$

We say that $\mathbf{v} \in V$ is a (strong) local minimizer of \mathcal{F} if there exists $\eta > 0$ such that for all $\varphi \in V$ we have $\mathcal{F}(\mathbf{v} + \delta\varphi) \geq \mathcal{F}(\mathbf{v})$ for all $\delta \in [0, \eta]$.

Remark 4.5. *The important property of the subdifferential to keep in mind here is that if $\mathbf{v} \in V$ is a local minimizer of a functional $\mathcal{F}: V \rightarrow \mathbb{R}$, then $\mathbf{0}_{\mathbf{L}^s(\Omega)} \in \partial\mathcal{F}(\mathbf{v})$. When \mathcal{F} is convex, the reverse of this statement is also true: if $\mathbf{0}_{\mathbf{L}^s(\Omega)} \in \partial\mathcal{F}(\mathbf{v})$, then \mathbf{v} is a local minimizer of \mathcal{F} .*

We write $\Psi: [0, \infty) \rightarrow \mathbb{R}$ the function given by

$$\Psi(a) = \begin{cases} \Phi_1(a) & \text{for all } a \leq 1, \\ \Phi_2(a) & \text{for all } a > 1, \end{cases} \quad (17)$$

where $\Phi_1, \Phi_2: [0, \infty) \rightarrow \mathbb{R}$ are primitives of $\frac{\phi_1}{2}$ and $\frac{\phi_2}{2}$ (cf. (9)) such that $\Phi_1(1) = \Phi_2(1) = 0$. We define the *dissipation* $\mathcal{D}: V \rightarrow \mathbb{R}$ by

$$\mathcal{D}(\mathbf{v}) = \int_{\Omega} \Psi(\|\mathbf{v} + \hat{\mathbf{u}}\|^2) \quad \text{for all } \mathbf{v} \in V.$$

Thanks to our assumptions on ϕ_1 and ϕ_2 we easily get that the domain of \mathcal{D} is indeed all of V , and it is thus a well-defined functional from V into \mathbb{R} . Consider the following problem: find $\mathbf{v} \in V$ such that there exists $\mathbf{g}_{\mathbf{v}} \in \partial\mathcal{D}(\mathbf{v})$ satisfying

$$\langle \mathbf{g}_{\mathbf{v}}, \varphi \rangle = \langle \mathbf{f}_0, \varphi \rangle \quad \text{for all } \varphi \in V. \quad (18)$$

The following result holds:

Lemma 4.6. *Any solution to Problem (18) is also solution to Problem (16).*

Proof. Suppose that $\mathbf{v} \in V$ is solution to Problem (18). Then we can pick $\mathbf{g}_{\mathbf{v}} \in \partial\mathcal{D}(\mathbf{v}) \subset \mathbf{L}^s(\Omega)$ so that (18) holds. By definition, for all $\varphi \in V$ we must have

$$\liminf_{\delta \rightarrow 0^+} \frac{\mathcal{D}(\mathbf{v} + \delta\varphi) - \mathcal{D}(\mathbf{v})}{\delta} \geq \langle \mathbf{g}_{\mathbf{v}}, \varphi \rangle.$$

Write V_1 the subset of V consisting of the functions which are supported in $\Omega_1(\mathbf{v} + \hat{\mathbf{u}})$. Then, for all $\varphi \in V_1$, since $-\varphi \in V_1$ as well, we get

$$\liminf_{\delta \rightarrow 0^+} \frac{1}{\delta} \int_{\Omega_1(\mathbf{v} + \hat{\mathbf{u}})} \left(\Psi(\|\mathbf{v} + \delta\varphi + \hat{\mathbf{u}}\|^2) - \Phi_1(\|\mathbf{v} + \hat{\mathbf{u}}\|^2) \right) \geq \langle \mathbf{g}_{\mathbf{v}}, \varphi \rangle$$

and

$$\liminf_{\delta \rightarrow 0^+} \frac{1}{\delta} \int_{\Omega_1(\mathbf{v} + \hat{\mathbf{u}})} \left(\Psi(\|\mathbf{v} - \delta\varphi + \hat{\mathbf{u}}\|^2) - \Phi_1(\|\mathbf{v} + \hat{\mathbf{u}}\|^2) \right) \geq -\langle \mathbf{g}_{\mathbf{v}}, \varphi \rangle,$$

which, by Lebesgue's dominated convergence theorem and the differentiability of Φ_1 , yield

$$\int_{\Omega} \Lambda_1(\mathbf{v} + \hat{\mathbf{u}}) \cdot \varphi = \int_{\Omega_1(\mathbf{v} + \hat{\mathbf{u}})} \phi_1(\|\mathbf{v} + \hat{\mathbf{u}}\|^2)(\mathbf{v} + \hat{\mathbf{u}}) \cdot \varphi \geq \langle \mathbf{g}_v, \varphi \rangle$$

and

$$-\int_{\Omega} \Lambda_1(\mathbf{v} + \hat{\mathbf{u}}) \cdot \varphi = -\int_{\Omega_1(\mathbf{v} + \hat{\mathbf{u}})} \phi_1(\|\mathbf{v} + \hat{\mathbf{u}}\|^2)(\mathbf{v} + \hat{\mathbf{u}}) \cdot \varphi \geq -\langle \mathbf{g}_v, \varphi \rangle.$$

All in all we get

$$\langle \mathbf{g}_v, \varphi \rangle = \langle \Lambda_1(\mathbf{v} + \hat{\mathbf{u}}), \varphi \rangle \quad \text{for all } \varphi \in V_1.$$

Similarly, denoting by V_2 the subset of V consisting of the functions which are supported in $\Omega_2(\mathbf{v} + \hat{\mathbf{u}})$, we get

$$\langle \mathbf{g}_v, \varphi \rangle = \langle \Lambda_2(\mathbf{v} + \hat{\mathbf{u}}), \varphi \rangle \quad \text{for all } \varphi \in V_2.$$

Thus the function defined by

$$\Lambda_v = \Lambda_1(\mathbf{v} + \hat{\mathbf{u}}) + \Lambda_2(\mathbf{v} + \hat{\mathbf{u}}) + \mathbf{g}_v \chi_{\Gamma(\mathbf{v} + \hat{\mathbf{u}})}$$

is such that $\langle \Lambda_v, \varphi \rangle = \langle \mathbf{g}_v, \varphi \rangle$ for all $\varphi \in V$. Therefore, from (18) we obtain

$$\langle \Lambda_v, \varphi \rangle = \langle \mathbf{f}_0, \varphi \rangle \quad \text{for all } \varphi \in V.$$

Moreover $\Lambda_v \in \Lambda(\mathbf{v} + \hat{\mathbf{u}})$, where we recall Λ is in (11). Hence \mathbf{v} is solution to Problem (16). \square

We now define the *energy* $\mathcal{E}: V \rightarrow \mathbb{R}$ associated to \mathcal{D} by

$$\mathcal{E}(\mathbf{v}) = \mathcal{D}(\mathbf{v}) - \langle \mathbf{f}_0, \mathbf{v} + \hat{\mathbf{u}} \rangle \quad \text{for all } \mathbf{v} \in V. \quad (19)$$

Let us write $M_{\mathcal{E}} \subset V$ the, possibly empty, set of local minimizers of \mathcal{E} . Consider the following minimization problem: find $\mathbf{v} \in V$ such that

$$\mathbf{v} \in M_{\mathcal{E}}. \quad (20)$$

By Remark 4.5, any solution to Problem (20) is also solution to Problem (18); if \mathcal{E} is convex these problems are actually equivalent. By Lemma 4.6 it therefore suffices to find a solution to Problem (20) in order to get the desired existence result on our original problem given in (14). The rest of this section will thus be solely dedicated to solving Problem (20).

4.3 Case $\lambda_1 \leq \lambda_2$

The result we wish to show here is the following:

Theorem 4.7 (Existence and uniqueness when $\lambda_1 \leq \lambda_2$). *Suppose that $\lambda_1 \leq \lambda_2$. Then, Problem (20) has a unique solution.*

Proof. Let us prove that the integrand $\Psi \circ \|\cdot\|^2$ (cf. (17)) of \mathcal{D} is strictly convex. Define the functions $\bar{\Phi}_1, \bar{\Phi}_2: [0, \infty) \rightarrow \mathbb{R}$ by

$$\bar{\Phi}_1(a) = \begin{cases} \Phi_1(a) & \text{for all } a \leq 1, \\ \frac{\lambda_1}{2}(a-1) & \text{for all } a > 1, \end{cases} \quad \text{and} \quad \bar{\Phi}_2(a) = \begin{cases} \frac{\lambda_2}{2}(a-1) & \text{for all } a \leq 1, \\ \Phi_2(a) & \text{for all } a > 1. \end{cases}$$

Then $\bar{\Phi}_1$ and $\bar{\Phi}_2$ are differentiable with

$$\bar{\Phi}'_1(a) = \frac{1}{2} \begin{cases} \phi_1(a) & \text{for all } a \leq 1, \\ \lambda_1 & \text{for all } a > 1, \end{cases} \quad \text{and} \quad \bar{\Phi}'_2(a) = \frac{1}{2} \begin{cases} \lambda_2 & \text{for all } a \leq 1, \\ \phi_2(a) & \text{for all } a > 1. \end{cases}$$

Since ϕ_1 and ϕ_2 are increasing on $[0, 1]$ and $[1, \infty)$, respectively, and $\phi_1(1) = \lambda_1$ and $\phi_2(1) = \lambda_2$, the derivatives $\bar{\Phi}'_1$ and $\bar{\Phi}'_2$ are also increasing so that $\bar{\Phi}_1$ and $\bar{\Phi}_2$ are convex. Furthermore, because $\lambda_1 \leq \lambda_2$ and ϕ_2 is increasing, we have $\bar{\Phi}'_2(a) \geq \bar{\Phi}'_1(a)$ for all $a > 1$; thus, the fact that $\bar{\Phi}_1(1) = \bar{\Phi}_2(1)$ (and so $\bar{\Phi}_1(1) = \bar{\Phi}_2(1)$) yields $\bar{\Phi}_1(a) \leq \bar{\Phi}_2(a)$ for all $a > 1$. Similarly, we get that $\bar{\Phi}_1(a) \geq \bar{\Phi}_2(a)$ for all $a < 1$. Let $a, b \in [0, \infty)$ and $t \in [0, 1]$. If $a, b \leq 1$, then $(1-t)a + tb \leq 1$ and

$$\begin{aligned} \Psi((1-t)a + tb) &= \bar{\Phi}_1((1-t)a + tb) = \bar{\Phi}_1((1-t)a + tb) \\ &\leq (1-t)\bar{\Phi}_1(a) + t\bar{\Phi}_1(b) = (1-t)\Psi(a) + t\Psi(b), \end{aligned}$$

and similarly if $a, b > 1$. If now $a \leq 1$, $b > 1$ and $(1-t)a + tb \leq 1$, then we have

$$\begin{aligned} \Psi((1-t)a + tb) &= \bar{\Phi}_1((1-t)a + tb) = \bar{\Phi}_1((1-t)a + tb) \\ &\leq (1-t)\bar{\Phi}_1(a) + t\bar{\Phi}_1(b) \leq (1-t)\bar{\Phi}_1(a) + t\bar{\Phi}_2(b) = (1-t)\Psi(a) + t\Psi(b), \end{aligned}$$

and similarly if $(1-t)a + tb > 1$ or $a > 1$ and $b \leq 1$. In all cases, we see that

$$\Psi((1-t)a + tb) \leq (1-t)\Psi(a) + t\Psi(b),$$

so that Ψ is convex. Note that one could reach the same conclusion using that

$$\Psi(a) = \max(\bar{\Phi}_1(a), \bar{\Phi}_2(a)) \quad \text{for all } a \geq 0.$$

Since ϕ_1 and ϕ_2 are positive on $(0, 1)$ and $[1, \infty)$, respectively, we get that Ψ is increasing. Therefore, the function $\Psi \circ \|\cdot\|^2$ is strictly convex.

We now want to use the direct method of the calculus of variations to show that \mathcal{E} has in fact a unique global (and thus local) minimizer. Let $(\mathbf{v}_n)_{n \in \mathbb{N}} \subset V$ be a minimizing sequence for \mathcal{E} . Then we know there exists $N \in \mathbb{N}$ large enough and $K > 0$ such that $\mathcal{E}(\mathbf{v}_n) < K$ for all $n > N$. Without loss of generality we can therefore assume that the sequence $(\mathcal{E}(\mathbf{v}_n))_{n \in \mathbb{N}}$ is bounded by some constant $K > 0$. Hence, thanks to the left-hand inequality in (10), for all $n \in \mathbb{N}$ we have

$$\begin{aligned} K > \mathcal{E}(\mathbf{v}_n) &= \int_{\Omega_1(\mathbf{v}_n + \hat{\mathbf{u}})} \Phi_1(\|\mathbf{v}_n + \hat{\mathbf{u}}\|^2) + \int_{\Omega_2(\mathbf{v}_n + \hat{\mathbf{u}})} \Phi_2(\|\mathbf{v}_n + \hat{\mathbf{u}}\|^2) - \int_{\Omega} \mathbf{f}_0 \cdot (\mathbf{v}_n + \hat{\mathbf{u}}) \\ &\geq \Phi_1(0) |\Omega| + \frac{c}{r} \int_{\Omega_2(\mathbf{v}_n + \hat{\mathbf{u}})} \|\mathbf{v}_n + \hat{\mathbf{u}}\|^r - \|\mathbf{f}_0\|_{L^s(\Omega)}^s \|\mathbf{v}_n + \hat{\mathbf{u}}\|_{L^r(\Omega)}^r \\ &\geq \left(\Phi_1(0) - \frac{c}{r} \right) |\Omega| + \frac{c}{r} \|\mathbf{v}_n + \hat{\mathbf{u}}\|_{L^r(\Omega)}^r - \|\mathbf{f}_0\|_{L^s(\Omega)} \|\mathbf{v}_n + \hat{\mathbf{u}}\|_{L^r(\Omega)}, \end{aligned}$$

which shows that the sequence $(\|\mathbf{v}_n\|_{L^r(\Omega)})_{n \in \mathbb{N}}$ is bounded. Thus we can extract a subsequence from $(\mathbf{v}_n)_{n \in \mathbb{N}}$, still denoted $(\mathbf{v}_n)_{n \in \mathbb{N}}$ which converges weakly to some $\mathbf{v} \in L^r(\Omega)$. Since further V is weakly closed we in fact have $\mathbf{v} \in V$. Because $\Psi \circ \|\cdot\|^2$ is convex, the dissipation \mathcal{D} is weakly lower semi-continuous and so is the energy \mathcal{E} . We therefore yield

$$\inf_{\mathbf{w} \in V} \mathcal{E}(\mathbf{w}) = \liminf_{n \rightarrow \infty} \mathcal{E}(\mathbf{v}_n) \geq \mathcal{E}(\mathbf{v}) \geq \inf_{\mathbf{w} \in V} \mathcal{E}(\mathbf{w}),$$

so that $\mathcal{E}(\mathbf{v}) = \inf_{\mathbf{w} \in V} \mathcal{E}(\mathbf{w})$ and \mathbf{v} is a global minimizer of \mathcal{E} and so $\mathbf{v} \in M_{\mathcal{E}}$.

To show that $M_{\mathcal{E}}$ is a singleton it is enough to prove that \mathcal{E} is strictly convex. Let $\mathbf{v}, \mathbf{w} \in V$ and $t \in (0, 1)$. Suppose furthermore that $\mathbf{v} \neq \mathbf{w}$ and write $A \subset \Omega$ the set where \mathbf{v} and \mathbf{w} are different; the Lebesgue measure of A is therefore positive. Note that we must have $\Psi(a) \neq 0$ for all $a \neq 1$. Using the strict convexity of $\Psi \circ \|\cdot\|^2$ we therefore get

$$\begin{aligned}
\mathcal{D}((1-t)\mathbf{v} + t\mathbf{w}) &= \int_{\Omega} \Psi(\|(1-t)\mathbf{v} + t\mathbf{w} + \hat{\mathbf{u}}\|^2) = \int_{\Omega} \Psi(\|(1-t)(\mathbf{v} + \hat{\mathbf{u}}) + t(\mathbf{w} + \hat{\mathbf{u}})\|^2) \\
&= (1-t) \int_{\Omega \setminus A} \Psi(\|\mathbf{v} + \hat{\mathbf{u}}\|^2) + t \int_{\Omega \setminus A} \Psi(\|\mathbf{w} + \hat{\mathbf{u}}\|^2) \\
&\quad + \int_A \Psi(\|(1-t)(\mathbf{v} + \hat{\mathbf{u}}) + t(\mathbf{w} + \hat{\mathbf{u}})\|^2) \\
&< (1-t) \int_{\Omega \setminus A} \Psi(\|\mathbf{v} + \hat{\mathbf{u}}\|^2) + t \int_{\Omega \setminus A} \Psi(\|\mathbf{w} + \hat{\mathbf{u}}\|^2) \\
&\quad + (1-t) \int_A \Psi(\|\mathbf{v} + \hat{\mathbf{u}}\|^2) + t \int_A \Psi(\|\mathbf{w} + \hat{\mathbf{u}}\|^2) \\
&= (1-t) \int_{\Omega} \Psi(\|\mathbf{v} + \hat{\mathbf{u}}\|^2) + t \int_{\Omega} \Psi(\|\mathbf{w} + \hat{\mathbf{u}}\|^2) = (1-t)\mathcal{D}(\mathbf{v}) + t\mathcal{D}(\mathbf{w}),
\end{aligned}$$

so that the dissipation \mathcal{D} is strictly convex. Consequently, the energy \mathcal{E} is also strictly convex and the proof is over. \square

4.4 Case $\lambda_1 > \lambda_2$

This case is more difficult to tackle than the case $\lambda_1 \leq \lambda_2$. Indeed, we lose the convexity of the integrand $\Psi \circ \|\cdot\|^2$ (cf. proof of Theorem 4.7), which by Tonelli's theorem of functional analysis means that \mathcal{E} is *not* weakly lower semi-continuous. As a consequence we cannot use the direct method of the calculus of variations in the weak topology to deduce the existence of a minimizer of \mathcal{E} .

To simplify our task at this point, we shall restrict to the one-dimensional case (i.e., $d = 1$) and leave the higher-dimensional case for future investigation. The results we present here therefore apply to the numerical experiments we present below. The one-dimensional case is simpler since we can easily characterize the space V depending on the boundary conditions, as will be clear from the proof of the following theorem:

Theorem 4.8 (Existence and uniqueness when $\lambda_1 > \lambda_2$). *Let $d = 1$ and suppose that $\lambda_1 > \lambda_2$. If $\text{Vol}^0(\Sigma_{\mathbf{v}}) = 0$, then Problem (20) has a solution. If instead $\text{Vol}^0(\Sigma_{\mathbf{v}}) > 0$, then Problem (20) has a unique solution.*

Proof. Without loss of generality, take $\Omega = (0, 1)$.

Case $\text{Vol}^0(\Sigma_{\mathbf{v}}) = 0$. First note that here $\Sigma_{\mathbf{p}} = \{0, 1\}$. Let us characterize V in this case. To this end, note that any $\eta \in V$ with $\int_0^1 \eta = 0$ has a primitive in $W_0^{1,s}((0, 1))$; indeed, the function $\psi: (0, 1) \rightarrow \mathbb{R}$ defined by

$$\psi(x) = \int_0^x \eta \quad \text{for all } x \in (0, 1)$$

satisfies $\psi' = \eta$ and $\psi(0) = \psi(1) = 0$. Let now $v \in V$ and define $\eta \in V$ as

$$\eta(x) = v(x) - \int_0^1 v \quad \text{for all } x \in (0, 1),$$

so that obviously $\int_0^1 \eta = 0$. Write $\psi \in W_0^{1,s}((0, 1))$ a primitive of η and compute, for all $\varphi \in V$,

$$\int_0^1 \left(v - \int_0^1 v \right) \varphi = \int_0^1 \eta \varphi = \int_0^1 \psi' \varphi = 0.$$

Thus $v = \int_0^1 v$ and v is constant. Since constant functions clearly belong to V , this shows that V is in fact the set of all constant functions on $(0, 1)$ and we can identify V with \mathbb{R} .

This in particular means that the energy \mathcal{E} defined in (19) can be identified with the following function $E: \mathbb{R} \rightarrow \mathbb{R}$:

$$E(\alpha) = \int_0^1 \Psi((\alpha + \hat{u})^2) - \alpha \int_0^1 f_0 \quad \text{for all } \alpha \in \mathbb{R},$$

where we recall that Ψ is given in (17) and $\hat{u} := \hat{\mathbf{u}}$ is as in Lemma 4.2. We can use the direct method of the calculus of variations on E in the Euclidean topology in \mathbb{R} . Let $(\alpha_n)_{n \in \mathbb{N}} \subset \mathbb{R}$ be a minimizing sequence for E . Using a similar calculation as in the proof of Theorem 4.7, thanks to (10) we can show that $(\alpha_n)_{n \in \mathbb{N}}$ is bounded in \mathbb{R} . Therefore, there exists a subsequence of $(\alpha_n)_{n \in \mathbb{N}}$, still denoted by $(\alpha_n)_{n \in \mathbb{N}}$, converging to some $\alpha \in \mathbb{R}$. By continuity of Ψ and Fatou's lemma we get that E is lower semi-continuous on \mathbb{R} , so that

$$\inf_{\beta \in \mathbb{R}} E(\beta) = \liminf_{n \rightarrow \infty} E(\alpha_n) \geq E(\alpha) \geq \inf_{\beta \in \mathbb{R}} E(\beta),$$

showing that α is a global minimizer of E and the constant function α belongs to $M_{\mathcal{E}}$.

Case $\text{Vol}^0(\Sigma_v) > 0$. Note that here $\Sigma_p \in \{\emptyset\} \cup \{\{0\}\} \cup \{\{1\}\}$. Similarly to the previous case, let us characterize V . Note that any $v \in V$ has a primitive in $W_0^{1,s}((0, 1))$; indeed, the function $\psi: (0, 1) \rightarrow \mathbb{R}$ defined for all $x \in (0, 1)$ by

$$\begin{cases} \psi(x) = \int_0^x v - \int_0^1 \left(\int_0^y v \right) dy & \text{if } \Sigma_p = \emptyset, \\ \psi(x) = \int_0^x v - \int_0^1 v & \text{if } \Sigma_p = \{1\}, \\ \psi(x) = \int_0^x v & \text{if } \Sigma_p = \{0\}, \end{cases}$$

satisfies $\psi' = \eta$, and $\int_0^1 \psi = 0$ if $\Sigma_p = \emptyset$ and $\psi(x) = 0$ for $x \in \Sigma_p$ otherwise. Let $v \in V$, write ψ a primitive of v and compute, for all $\varphi \in V$,

$$\int_0^1 v \varphi = \int_0^1 \psi' \varphi = 0,$$

so that $v = 0$. This shows that $V = \{0\}$, i.e., V contains only the zero function on $(0, 1)$. Trivially then, the zero function is the unique global minimizer of the energy \mathcal{E} in (19) and $M_{\mathcal{E}}$ is a singleton. Note that in this case the energy is only trivially convex. \square

5 Numerical approximation

In this part we present the numerical approximation for the considered problem when $d = 1$; we will still keep boldfaced notation for vectors and vector-valued functions for coherence with most of the previous sections. In particular, in Section 5.1 the algorithm to track the interface is described. Later in Section 5.2 we describe the discretization adopted for a known interface. As mentioned in the introduction, for the implementation we have used the flexible framework of the PorePy library; see [32].

We introduce a mesh Ω_h composed of non-overlapping segments $E \in \Omega_h$ that approximate Ω ; we clearly have $\overline{\Omega}_h = \cup_{E \in \Omega_h} \overline{E}$. At the discrete level we can define the approximate configuration \mathcal{C}_h which is given by the set $\mathcal{C}_h = \{\Omega_{1,h}, \Omega_{2,h}, \Gamma_h\}$, where respectively $\Omega_{1,h} \subset \Omega_h$ and $\Omega_{2,h} \subset \Omega_h$ are the approximations of the domains Ω_1 and Ω_2 . Γ_h is the approximation of the interface Γ . Note that for simplicity we are dropping the dependence of these regions on the velocity field. For each element E we name e_1 and e_2 its two extremal vertices and h_E its length. We let $h = \max_{E \in \Omega_h} h_E$ be the mesh size. When more than one fracture is present, each intersection is respected by the grid. We indicate by (\mathbf{u}_h, p_h) the approximation of (\mathbf{u}, p) for a given mesh.

5.1 Interface tracking algorithm

We suppose that the equations are discretized with a numerical scheme that gives an accurate enough velocity field. We consider an iterative scheme such that for each step i a tentative configuration $\mathcal{C}_h^{(i)}$ approximates \mathcal{C}_h . For a given configuration $\mathcal{C}_h^{(i-1)}$, the proposed algorithm solves the differential problem obtaining a new velocity field $\mathbf{u}^{(i)}$. To speed up the computation, we evaluate condition (5) only at the extremities of each grid element E . If we obtain opposite values, we can thus determine the position of an interface in the considered element up to a given tolerance ϵ_Γ . This part can be coded with an embarrassingly parallel workload, speeding up the algorithm. Having checked all the elements and computed the new configuration $\mathcal{C}_h^{(i)}$, the algorithm resets with the new configuration as starting point. The exit strategy considers the position of Γ_h for two successive iterations: if their distance is smaller than a given threshold ϵ_Ω , then a stable configuration is reached and the algorithm ends. We summarize in Algorithm 1 the implemented scheme.

We see that with this algorithm we cannot locate multiple interfaces in a single element E ; this is a direct implication of the fact that $\Omega_{1,h}^{(i)}$ or $\Omega_{2,h}^{(i)}$ would be smaller than the mesh size in this case. The algorithm is also unable to track interfaces which are full-dimensional (in this case of space dimension 1) since we choose to place only one point as the interface within an element whose vertices have velocities around the threshold speed.

To avoid unnecessary loops due to the chosen accuracy, numerical experiments showed that a good value of ϵ_Ω is comparable with the mesh size given at the outset of the problem. Also, the value of ϵ_Γ is set quite small to determine the interfaces with high precision. Numerical examples when the interface inverse permeability jump is non-positive indicated convergence of the proposed scheme, independently from the starting configuration, thus suggesting that the problem has a unique solution and that, in line with Remark 3.3, the interface should not be full-dimensional.

Algorithm 1: Interface tracking algorithm.

Data: For $i = 1$: the configuration $\mathcal{C}_h^{(i-1)}$ and the tolerances $(\epsilon_\Gamma, \epsilon_\Omega)$;

Result: For $i = \text{end}$: the configuration $\mathcal{C}_h^{(i)}$;

```
do
   $(\mathbf{u}^{(i)}, p^{(i)}) \leftarrow \text{PDE}(\mathcal{C}_h^{(i-1)});$ 
  for  $E = (e_1, e_2) \in \Omega_h^{(i-1)}$  do
     $(c_1, c_2) \leftarrow (\|\mathbf{u}^{(i)}(e_1)\| < 1, \|\mathbf{u}^{(i)}(e_2)\| < 1);$ 
    if  $c_1 \neq c_2$  then
       $\mathcal{C}_h^{(i)} \text{ in } E \leftarrow \text{Interface}(\mathbf{u}^{(i)});$ 
    end
  end
   $d \leftarrow \text{Distance}(\Gamma_h^{(i)}, \Gamma_h^{(i-1)});$ 
   $i \leftarrow i + 1;$ 
while  $d > \epsilon_\Omega;$ 
```

5.2 Discretization in space

Following the algorithm discussed before, we assume that a configuration $\mathcal{C}_h^{(i)}$ is given. In the case of non-linear constitutive relations $\mathbf{\Lambda}$ an iterative scheme can be used, e.g., Picard or Newton or L-scheme. The solution is computed up to a tolerance ϵ_{n1} . In our implementation we have considered a Picard iteration scheme. For this, to discuss the numerical approximation, we assume thus a linear constitutive relation $\mathbf{\Lambda}$.

Following [25], to solve the problem we consider the mixed finite element approximation of lowest-order degree. For a given mesh Ω_h we have $(\mathbf{u}_h, p_h) \in (\mathbb{P}_0(\Omega_h), \mathbb{RT}_0(\Omega_h))$, where the first is the space of constant piecewise polynomial and the second the Raviart–Thomas space; see [37, 38]. This pair of discrete spaces is stable and gives a good approximation for the velocity field, essential for our purposes. The resulting discrete problem is well-posed, see also [14, 25], and the discrete solution converges to the exact one as h goes to zero.

6 Numerical examples

In this part, we present numerical evidence for the quality and effectiveness of the previously introduced framework. Particularly for increasing geometrical and physical complexity. We consider three cases, starting from a single fracture in Section 6.1, two crossing fractures in Section 6.2, and concluding with the fracture network of Benchmark 1 from [24] in Section 6.3. In all cases, linear and non-linear velocity-pressure relations are considered as well as the impact of a possible vector source term \mathbf{f} . The threshold on the velocity norm is set as $\bar{u} = 0.15$, so that we have

$$\Omega_1 = \{\mathbf{x} \in \Omega \mid \|\mathbf{u}(\mathbf{x})\| < \bar{u}\} \quad \Omega_2 = \{\mathbf{x} \in \Omega \mid \|\mathbf{u}(\mathbf{x})\| > \bar{u}\} \quad \Gamma = \{\mathbf{x} \in \Omega \mid \|\mathbf{u}(\mathbf{x})\| = \bar{u}\}.$$

If not otherwise specified, we consider a mesh size equal to $h = 5 \cdot 10^{-2}$ as well as $\epsilon_\Omega = h$; the maximum number of iterations to reach a stable configuration with Algorithm 1 is set to 50; and to track the interface we set $\epsilon_\Gamma = 10^{-10}$. In all the cases, the initial configuration is chosen to be $\Omega_1^{(0)} = \Omega$, i.e., the whole domain coincides with the low-speed region.

Our simulations, unless mentioned otherwise, are based on the following combinations of laws. In the linear case, we consider a combination of classical Darcy laws between the velocity and pressure, namely $\mathbf{K}^{-1}\mathbf{u} = -\nabla p + \mathbf{f}$ with $\mathbf{K} = k\mathbf{I}$, where \mathbf{I} is the identity matrix and

$$k = \begin{cases} k_1 = 1 & \text{in } \Omega_1, \\ k_2 = 10 & \text{in } \Omega_2. \end{cases}$$

Specifically, we have

$$\mathbf{\Lambda}(\mathbf{u}) = \begin{cases} \mathbf{u} & \text{in } \Omega_1, \\ 0.1\mathbf{u} & \text{in } \Omega_2. \end{cases} \quad (21)$$

When the non-linear case is studied, a non-linear and heterogeneous relationship between the velocity and the pressure is set. We assume a linear Darcy flow in Ω_1 and a Darcy–Forchheimer flow in Ω_2 . Specifically, we have

$$\mathbf{\Lambda}(\mathbf{u}) = \begin{cases} \mathbf{u} & \text{in } \Omega_1, \\ (0.01 + 3\|\mathbf{u}\|)\mathbf{u} & \text{in } \Omega_2. \end{cases} \quad (22)$$

If not specified, we consider 50 as maximum for the number of iterations of the non-linear solver with tolerance ϵ_{n1} equal to 10^{-4} .

These examples were developed with the open source library PorePy [32]. The associated scripts are freely accessible. PorePy uses Gmsh [31] to construct the grids.

6.1 Single fracture network

In this first case, we consider a single fracture $\Omega = (0, 1)$. Boundary conditions are set to zero for the pressure. In the sequel, we consider a linear and non-linear law relationship between \mathbf{u} and p . The scalar and vector source terms are set equal to

$$q(\mathbf{x}) = \begin{cases} 1 & \text{if } x_1 \leq 0.3, \\ -1 & \text{if } 0.3 < x_1 < 0.7, \\ 1 & \text{if } x_1 \geq 0.7, \end{cases} \quad \text{and} \quad \mathbf{f} = [5 \cdot 10^{-2}, 0, 0]^\top.$$

6.1.1 Linear case. In this part, we consider the linear case with $\mathbf{\Lambda}$ as in (21). The numerical solution is reported in Figure 1 along with some snapshots of the tentative solutions from Algorithm 1. What the “if Ω_1 ” legend represents is a binary outcome saying if the region is Ω_1 or not. The ”condition” legend represents the configuration at the previous algorithm iteration. The first figure gives the initial condition imposed, the second the configuration after 3 steps and the third the final solution (at iteration 6). We notice the creation of multiple interfaces Γ , which might change during the determination of the final configuration. By changing the initial condition we get to the same stationary solution, and by refining the grid we obtain a stable outcome similar to the one presented in Figure 1.

In Figures 2 and 3 we study a case different from (21), where we test our algorithm for various permeabilities k_2 while fixing $k_1 = 1$. By increasing the maximum number of iterations to 1000, Figure 2 on the left shows the impact of changing k_2 on the number of iterations for the Algorithm 1. We see that for $k_2 \geq k_1$ the solution is always computable while we cannot draw the same conclusion for $k_2 < k_1$. In this latter case, the algorithm “jumps” between

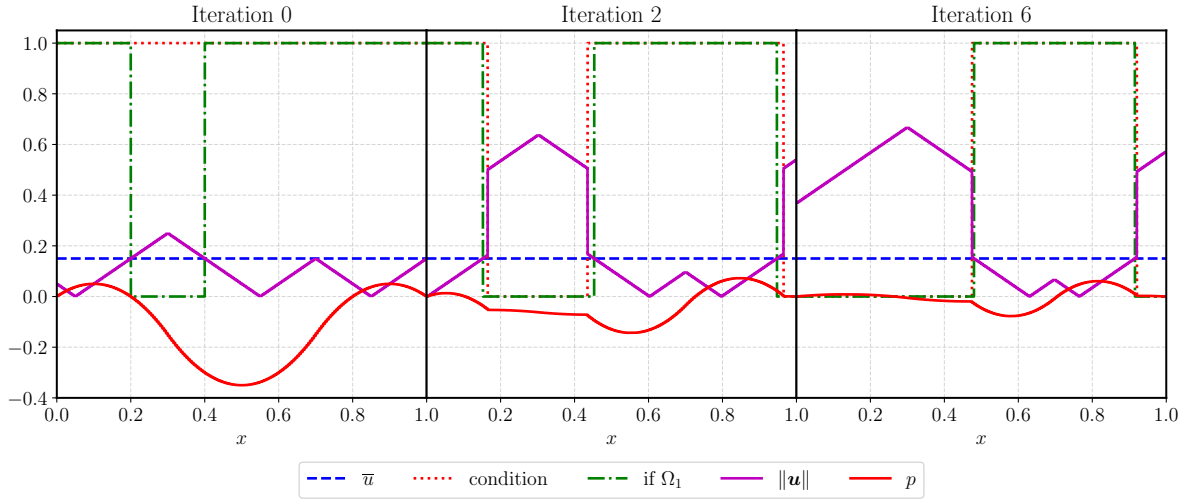


Figure 1: Solution for different iterations for the problem of Section 6.1.1. From the left at iteration 0, 2, and 6. The green line represents if the portion of the fracture belongs to Ω_1 or not. The pressure profile is amplified by a factor of 10.

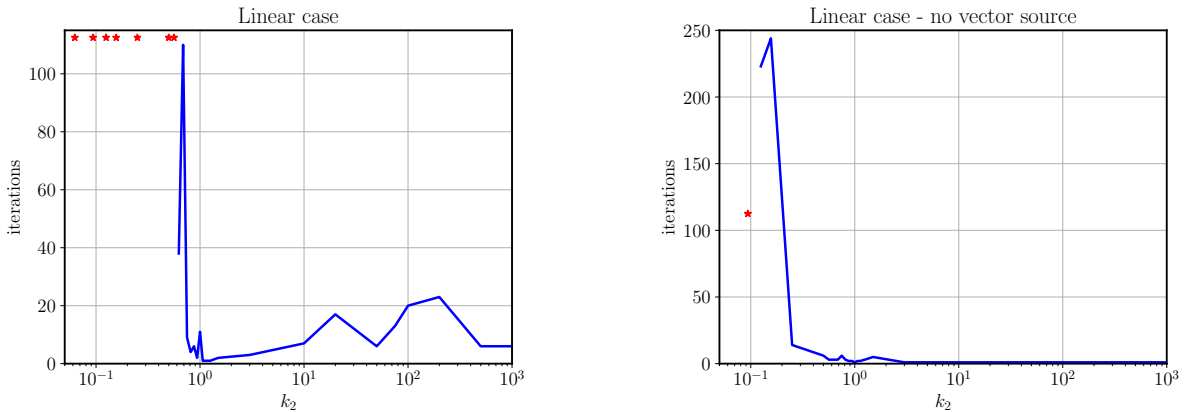


Figure 2: Number of iterations of Algorithm 1 for different values of k_2 for the example in Section 6.1.1. The red asterisks mean that the maximum number of iterations is reached.

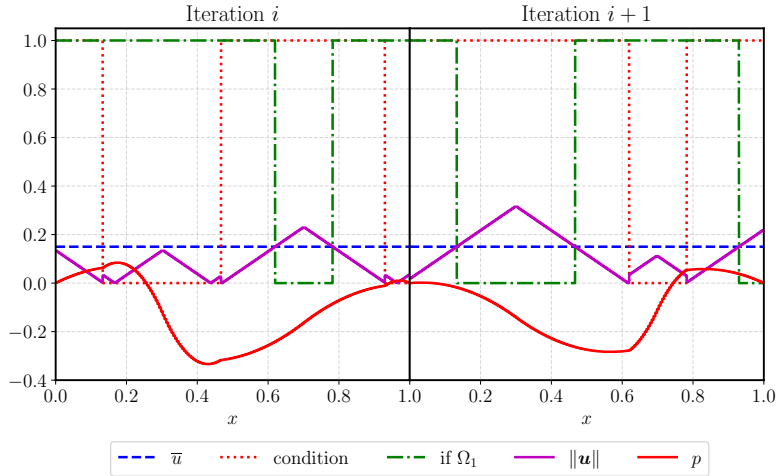


Figure 3: The two solutions computed by the algorithm for $k_2 = 0.5625$; see Section 6.1.1.

ϵ_{nl}	it_{out}	it_{in}	err_p	err_u
10^{-1}	2	3	$1.2 \cdot 10^{-5}$	$8.7 \cdot 10^{-6}$
10^{-2}	2	4	$1.8 \cdot 10^{-7}$	$1.3 \cdot 10^{-7}$
10^{-3}	2	5	$2.8 \cdot 10^{-9}$	$2.2 \cdot 10^{-9}$
10^{-4}	2	6	$4.4 \cdot 10^{-11}$	$2.1 \cdot 10^{-11}$
10^{-5}	2	7	$2.4 \cdot 10^{-12}$	$1.0 \cdot 10^{-11}$
10^{-8}	2	11	0	0
10^{-12}	2	15	—	—

Table 1: Numbers of iterations and errors computed for the example in Section 6.1.2.

the two states and thus does not converge. An example, for $k_2 = 0.5625$ is shown in Figure 3, where we notice that “if Ω_1 ” and “condition” are perfectly flipped in any two successive iterations.

By setting $\mathbf{f} = \mathbf{0}$ and $p(1) = 0.2$, the latter to avoid that the algorithm converges in 1 iteration for each value of k_2 , we can do the same analysis and obtain the plot in Figure 2 on the right. We deduce that the presence of the vector source has an impact on the computability of the solution when $k_2 > k_1$, that is, when the interface permeability jump is positive.

We can conclude that, even in this simple setting, the obtained numerical evidence is interesting and gives a valid support to the developed theory, at least when $k_2 \geq k_1$.

6.1.2 Non-linear case. In this part, we consider the non-linear case with Λ as in (22). Figure 4 shows the numerical solution obtained at different iteration steps of Algorithm 1. The stable solution is reached very quickly and only two iterations of the outer scheme are needed. We see the effect on the pressure of the non-linear law, which changes shape between the initial configuration and iteration 1. By changing the parameters, it is possible to show that the obtained solution is independent from the initial condition and stable with respect the grid refinement, once the mesh size is small enough to separate close interfaces. In this case 2 iterations are needed to reach the stable solution, the first requires only 1 iteration and the second 6.

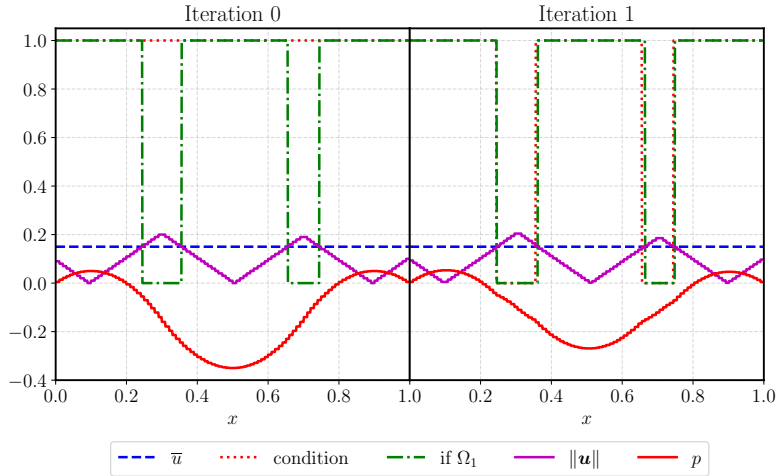


Figure 4: Solution for different iterations for the problem of Section 6.1.2. From the left at iteration 0, 1. The green line represents if the portion of the fracture belongs to Ω_1 or not. The pressure profile is amplified by a factor of 100.

We consider now the effect of the tolerance imposed in the non-linear solver ϵ_{nl} , in particular its effect on the number of iterations and resulting error. By keeping fixed the spatial discretization, we compute a reference solution $(\mathbf{u}_{\text{ref}}, p_{\text{ref}})$ with tolerance $\epsilon_{\text{nl}} = 10^{-12}$. We report in Table 1 the comparison with higher tolerances. In all cases the first iteration requires only two non-linear cycles, since the initial configuration has only a linear problem. At the second iteration the non-linear steps depend on the chosen tolerance, this value is reported in the table. In particular, we notice that both errors err_p for p and err_u for \mathbf{u} computed as

$$\text{err}_p = \frac{\|p_{\text{ref}} - p\|}{\|p_{\text{ref}}\|} \quad \text{and} \quad \text{err}_u = \frac{\|\mathbf{u}_{\text{ref}} - \mathbf{u}\|}{\|\mathbf{u}_{\text{ref}}\|}$$

have a monotone decay. The norms in the previous expression are the Euclidean norms of the solution vector. The error is rather small and decays very quickly, reaching zero for the non-linear tolerance equal to 10^{-3} . The outer iterations are not influenced by this parameters, probably due to the small errors obtained in all the cases.

Also in this case we can conclude that, even in this simple setting, the obtained numerical evidence is interesting and gives a valid support to the developed theory.

6.2 Crossing fractures

In this second case, we consider the domain made of two crossing fractures. We set $\Omega = \Omega_{\text{horiz}} \cup \Omega_{\text{vert}}$ where $\Omega_{\text{horiz}} = (0, 1) \times \{0.5\}$ and $\Omega_{\text{vert}} = \{0.5\} \times (0, 1)$; both Ω_{horiz} and Ω_{vert} are identifiable with $(0, 1)$. We consider a zero vector source term \mathbf{f} and a scalar source term given on Ω_{horiz} and Ω_{vert} respectively by

$$q_{\text{horiz}}(\mathbf{x}) = \begin{cases} 1 & \text{if } x_1 \leq 0.3 \\ -1 & \text{if } 0.3 < x_1 < 0.7 \\ 1 & \text{if } x_1 \geq 0.7 \end{cases} \quad \text{and} \quad q_{\text{vert}}(\mathbf{x}) = \begin{cases} 1 & \text{if } x_2 \leq 0.3 \\ -1 & \text{if } 0.3 < x_2 < 0.7 \\ 1 & \text{if } x_2 \geq 0.7 \end{cases}.$$

On the boundary we set $p(0, 0.5) = 0$ and $p(0.5, 0) = p(1, 0.5) = p(0.5, 1) = 0.1$.

6.2.1 Linear case. In this part, we consider the linear case with $\mathbf{\Lambda}$ as in (21). Figure 5 shows the graphical representation of the solution for both the horizontal and vertical part of Ω for all the iterations of Algorithm 1. We notice the influence of the crossing through a velocity jump in Ω_{horiz} , while the pressure profile is continuous as condition (8) imposes. Also in this case, by changing the initial condition we obtain the same final outcome, where all the domain becomes $\Omega_{2,h}$.

Also with this more complex case, the obtained numerical evidence is insightful and shows good properties for the developed approximation framework which is apparently applicable to fracture networks.

6.2.2 Non-linear case. In this part, we consider the non-linear case with $\mathbf{\Lambda}$ as in (22). The obtained numerical solution is reported in Figure 6. The scheme takes 5 iterations to converge with increasing number of non-linear solver iterations as (1, 6, 8, 9). The obtained solution shows that the high-speed model, being Darcy–Forchheimer, is more proper to describe most of the problem leaving the slow Darcian regime in the vicinity of the boundary where the non-zero pressure condition is imposed. It is important to note that the plots show the norm of \mathbf{u} which presents a jump only in the horizontal fracture. Nevertheless, condition (8) is respected at the fracture intersection since a velocity jump is also present in the other fracture. The representation of only $\|\mathbf{u}\|$ hides this details. By changing the initial condition or refining the mesh, we obtain again the same final outcome.

We can conclude that also in presence of a non-linear and heterogeneous law the proposed framework works properly on a network of fractures.

6.3 Multiple fracture network

We finally consider a complex fracture network, with geometry taken from Benchmark 1 of [24]. It is composed of 6 intersecting fractures as Figure 7 shows, along with the set of boundary conditions. We denote by Ω_s the set of smaller fracture branches, which will be useful in the following. Null and unitary vector and scalar sources are considered, respectively. As done with the previous examples, we will consider the linear and non-linear case in the next Sections.

6.3.1 Linear case. We consider here the same linear relations as in Section 6.1.1; see (21). The obtained solution is represented in Figure 8. The scheme converges after 4 iterations of Algorithm 1. We see an interesting result: $\Omega_{2,h}$, which is the high-velocity region, is automatically positioned on the main pathways between the inflow and outflow parts of the network. Again, the algorithm showed robustness when changing the initial configuration and refining the grid.

Even for this complex configuration, the proposed algorithm is capable to compute a reasonable solution with a limited cost.

6.3.2 Non-linear case. We consider in this part the non-linear case, where the constitutive law combination is given as

$$\mathbf{\Lambda}(\mathbf{u}) = \begin{cases} \mathbf{u} & \text{in } \Omega_1, \\ (0.01 + 0.25 \|\mathbf{u}\|)\mathbf{u} & \text{in } \Omega_2. \end{cases}$$

Algorithm 1 takes 4 steps to reach the final configuration with an average of 18 iterations of the non-linear solver for each step. Figure 9 shows the obtained numerical solution for different iterations. The obtained solution is again insightful, positioning the high-speed region, given

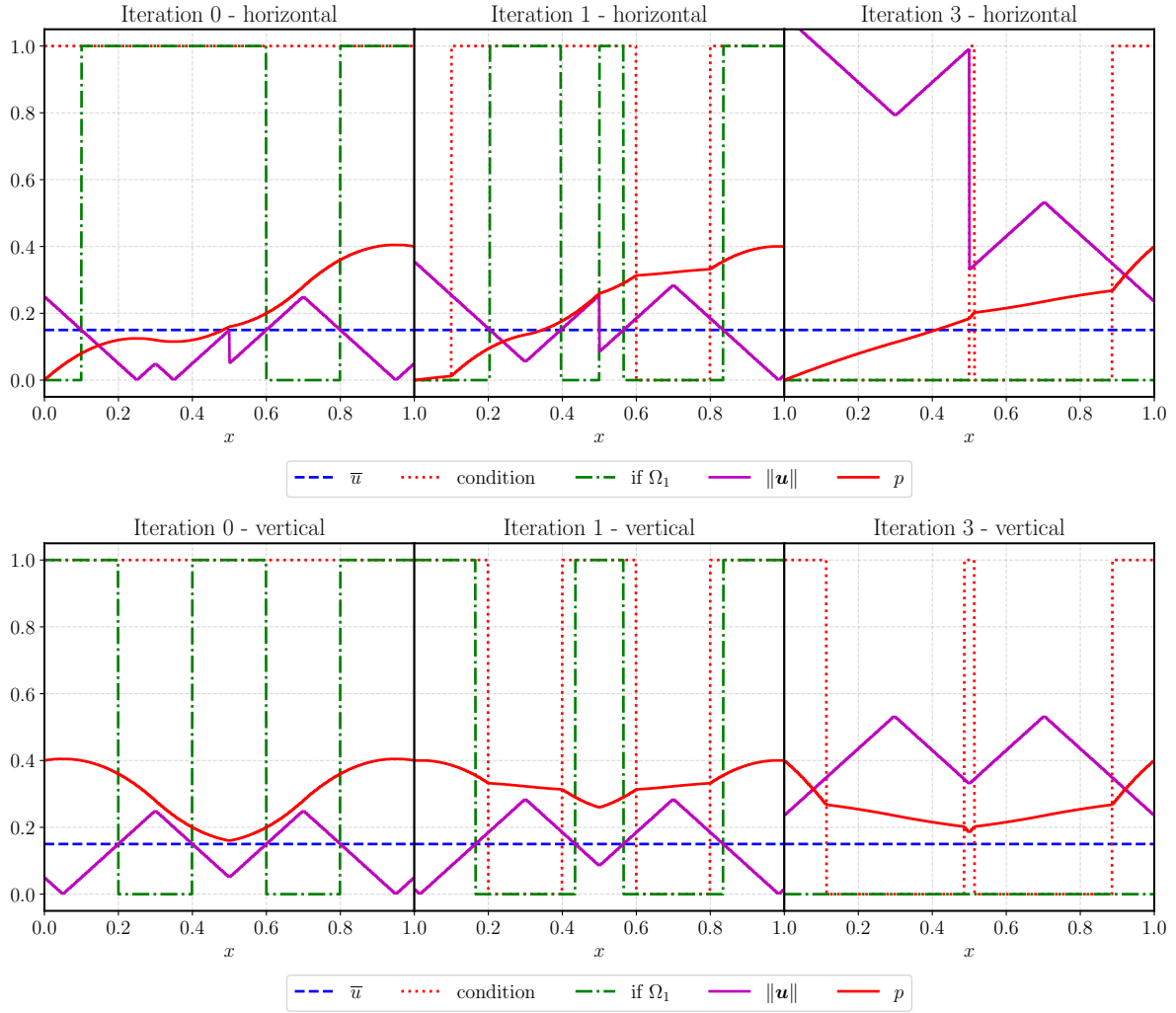


Figure 5: Solution for different iterations for the problem of Section 6.2.1. The pressure profile is amplified by a factor of 4. On the top for the horizontal part of Ω , while on the bottom for the vertical one.

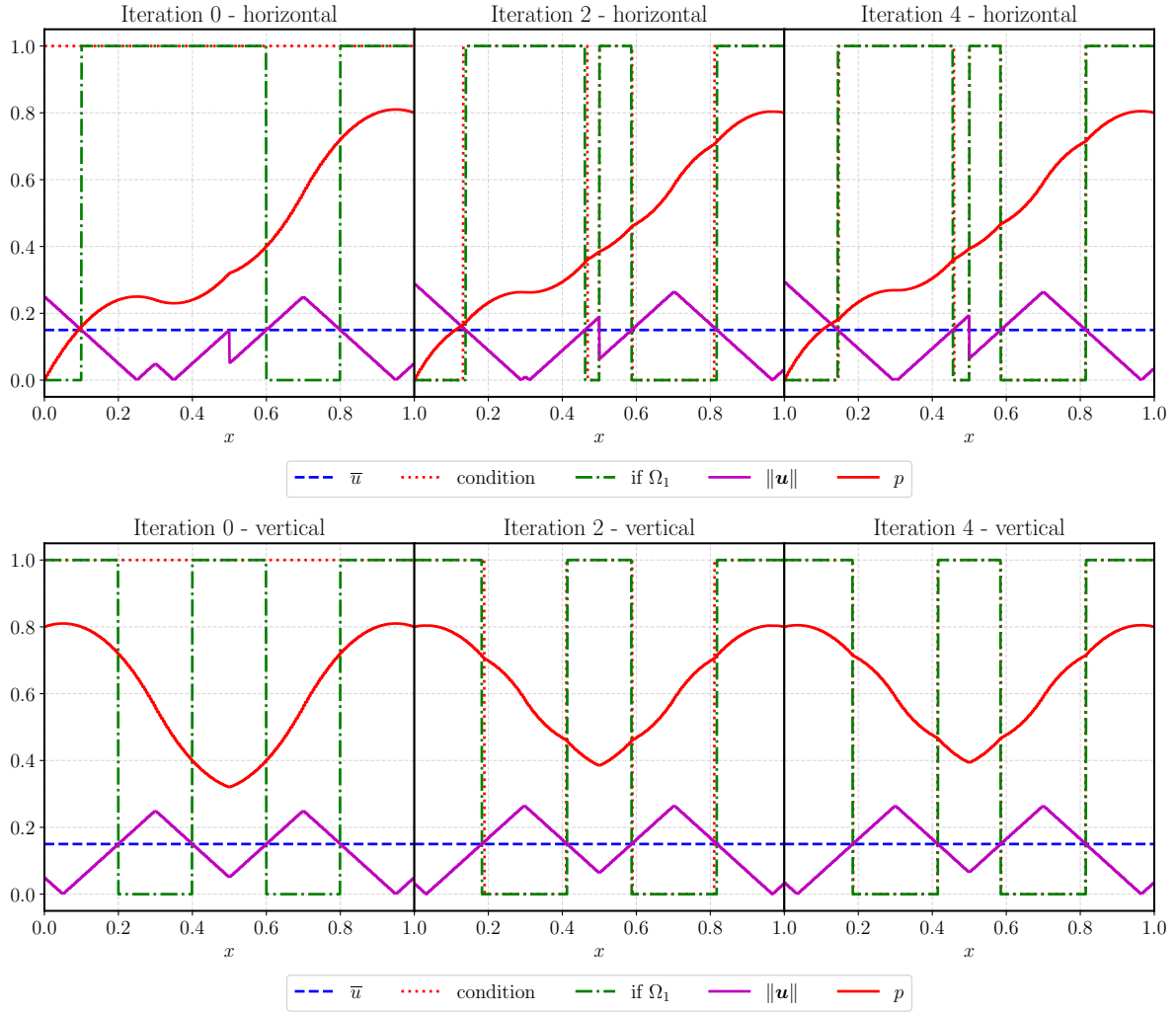


Figure 6: Solution for different iterations for the problem of Section 6.2.2. The pressure profile is amplified by a factor of 8. On the top for the horizontal part of Ω , while on the bottom for the vertical one.

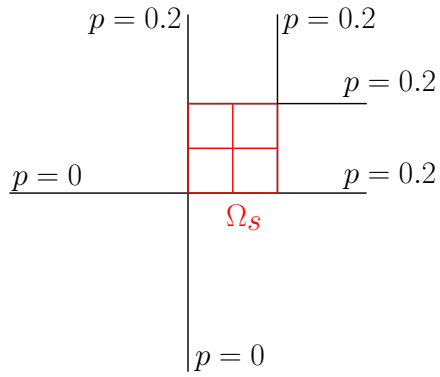


Figure 7: Representation of the fracture network for the examples in Section 6.3. We have reported the boundary conditions as well as the portion of the network with small branches in red Ω_s .

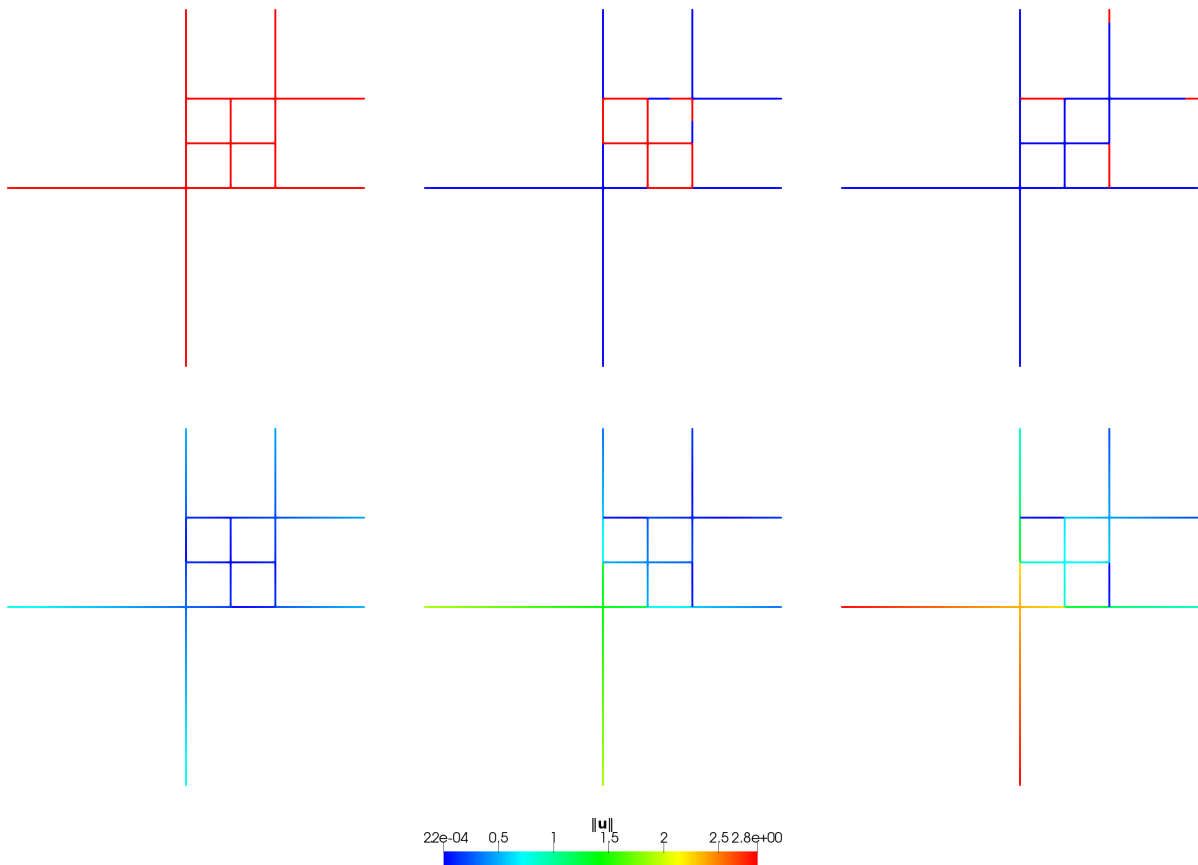


Figure 8: Solution for different iterations, respectively (0, 1, 4), for the problem of Section 6.3.1. On the top the condition “if Ω_1 ” is represented with red indicating “true” and blue “false”. On the bottom the norm of the velocity.

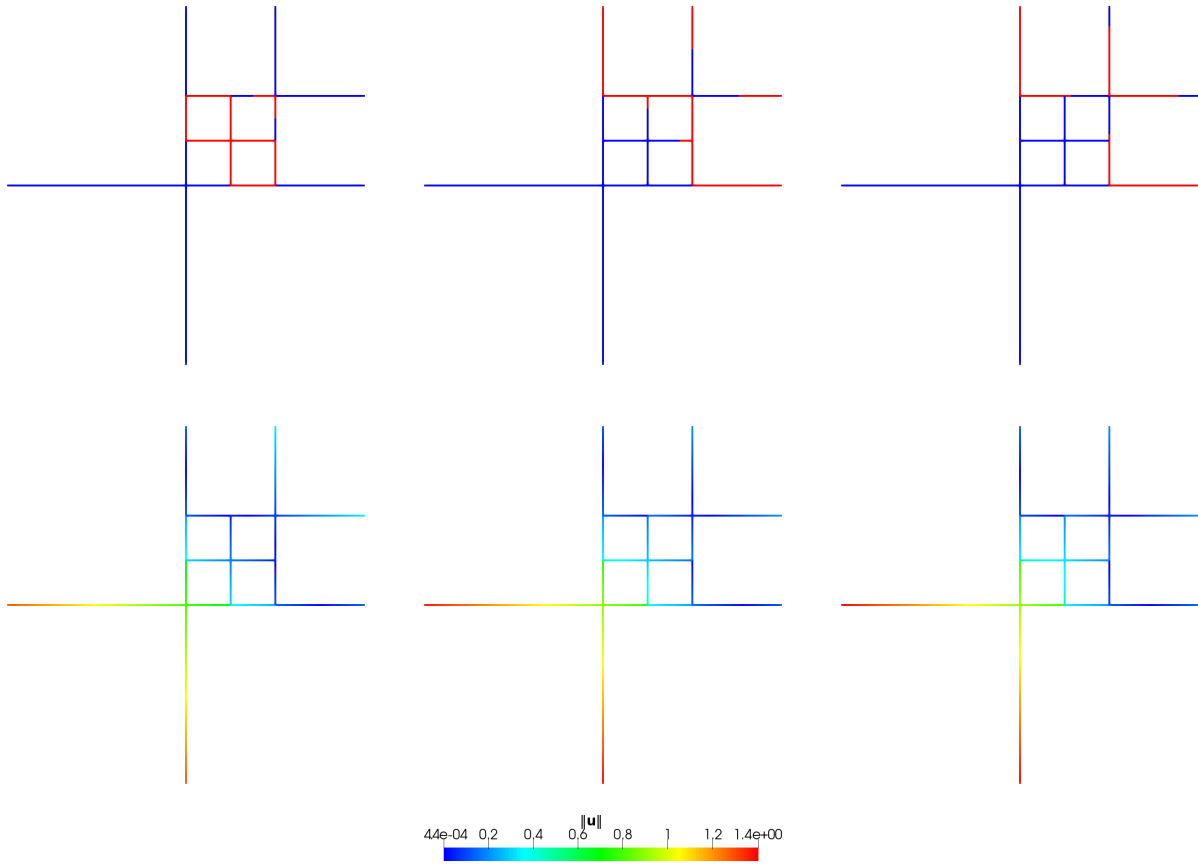


Figure 9: Solution for different iterations, respectively (1, 3, 4), for the problem of Section 6.3.2. On the top the condition "if Ω_1 " is represented with red indicating "true" and blue "false". On the bottom the norm of the velocity.

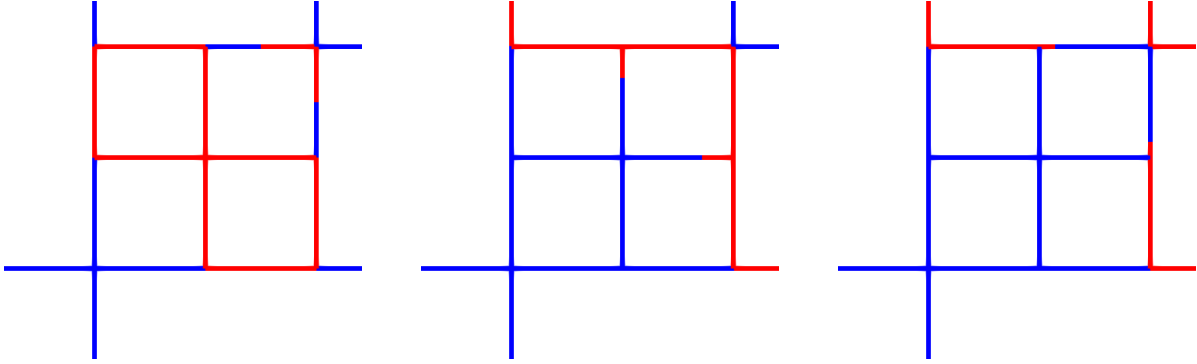


Figure 10: Zoom around the short fracture branches Ω_s of the “if Ω_1 ” condition for different iterations, respectively (1, 3, 4), for the problem of Section 6.3.2.

by $\Omega_{2,h}$, in the longest fracture branches and the low-speed region $\Omega_{1,h}$ mainly in the fracture branches at the outflow. There is a transition zone from $\Omega_{2,h}$ to $\Omega_{1,h}$ that mainly takes place in Ω_s . A zoom-in is reported in Figure 10 to better clarify the evolution of $\Omega_{2,h}$ and $\Omega_{1,h}$ at the small fracture branches.

This final example shows a very interesting and physically sound final configuration, which might have been hard to predict without the framework introduced in this work. All these examples showed the applicability and importance of the model adaptation and support the presented Algorithm 1 to be a valid approach for its solution.

7 Conclusion

In this work we introduced a new model for discrete fracture networks that is able to adapt the constitutive relation between velocity and pressure depending on the magnitude of the fluid velocity, which is part of the unknowns.

We presented a mathematical formulation for it, and with an energy argument we were able to show that under reasonable hypotheses on the constitutive law the problem has a solution. When the interface inverse permeability jump is non-negative, the problem is convex and we could show existence in any space dimension; when it is negative, however, the problem becomes non-convex and we had to restrict our proof of existence to one space dimension. We also introduced a discrete algorithm that, for a given problem, tracks the low- and high-speed regions as well at the interface separating them. We considered various constitutive relations for distinct parts of the network, such as the classical Darcy law and the non-linear Darcy–Forchheimer law. Several numerical examples showed the validity of the proposed approach by increasing the geometrical and physical complexity of the problem. We noticed that when the interface inverse permeability jump is positive, the algorithm seems not to converge and oscillate indefinitely between two configurations. In the complementary non-positive case, the algorithm seems to behave and converge nicely. Let us summarize these results:

From a modeling point of view, as mentioned in the introduction, future extensions will be the inclusion of the rock matrix and the possibility of having more than two constitutive laws for the problem.

From an analytical point of view, open questions include the existence of solutions when $d > 1$ and the interface inverse permeability jump is negative, and the extension of the existence results to tensor permeabilities when $d > 1$; see Remark 3.1. In addition, characterizing

	$\lambda_{21} > 0$	$\lambda_{21} = 0$	$\lambda_{21} < 0$
existence of solutions	yes	yes	yes if $d = 1$
convexity of energy	yes	yes	no*
convergence of algorithm ($d = 1$)	no	yes	yes

* unless in trivial case $d = 1$ and $\Sigma_v \neq \emptyset$

Table 2: Summary of results according to the interface inverse permeability jump $\lambda_{21} := \lambda_2 - \lambda_1$.

admissible constitutive laws on the interface (rather than leaving the choice as a free parameter of the model, as we did here) as well as determining the Hausdorff dimension of the interface are interesting questions that would allow us to study uniqueness of solutions.

From a numerical point of view, further extensions will be the the development of the tracking algorithm for $d > 1$ and the proof of its convergence when the interface inverse permeability jump is non-positive, and the development of an alternative algorithm when the jump is positive.

References

- [1] E. Ahmed, A. Fumagalli, and A. Budiša. A multiscale flux basis for mortar mixed discretizations of reduced Darcy–Forchheimer fracture models. *Computer Methods in Applied Mechanics and Engineering*, 354:16–36, 2019.
- [2] E. Ahmed, A. Fumagalli, A. Budiša, E. Keilegavlen, J. M. Nordbotten, and F. A. Radu. Robust linear domain decomposition schemes for reduced non-linear fracture flow models. Technical report, arXiv:1906.05831 [math.NA], 2019.
- [3] C. Alboin, J. Jaffré, J. E. Roberts, X. Wang, and C. Serres. Domain Decomposition for some Transmission Problems in Flow in Porous Media. In *Numerical treatment of multiphase flows in porous media (Beijing, 1999)*, volume 552 of *Lecture Notes in Phys.*, pages 22–34. Springer, Berlin, 2000.
- [4] L. Amir, M. Kern, V. Martin, and J. E. Roberts. Décomposition de domaine et préconditionnement pour un modèle 3D en milieu poreux fracturé. In *Proceeding of JANO 8, 8th conference on Numerical Analysis and Optimization*, Dec. 2005. 2005.
- [5] P. Angot, F. Boyer, and F. Hubert. Asymptotic and numerical modelling of flows in fractured porous media. *M2AN Mathematical Modelling and Numerical Analysis*, 43(2):239–275, 2009.
- [6] J. Audu, F. Fairag, and S. Messaoudi. On the well-posedness of generalized Darcy–Forchheimer equation. *Boundary Value Problems*, 2018, 2018.
- [7] M. F. Benedetto, A. Borio, and S. Scialò. Mixed virtual elements for discrete fracture network simulations. *Finite Elements in Analysis and Design*, 134:55–67, 2017.
- [8] I. Berre, W. M. Boon, B. Flemisch, A. Fumagalli, D. Gläser, E. Keilegavlen, A. Scotti, I. Stefansson, A. Tatomir, K. Brenner, S. Burbulla, P. Devloo, O. Duran, M. Favino, J. Hennicker, I.-H. Lee, K. Lipnikov, R. Masson, K. Mosthaf, M. G. C. Nestola, C.-F. Ni, K. Nikitin, P. Schädle, D. Svyatskiy, R. Yanbarisov, and P. Zulian. Verification

- benchmarks for single-phase flow in three-dimensional fractured porous media. *Advances in Water Resources*, 147, 2020.
- [9] I. Berre, F. Doster, and E. Keilegavlen. Flow in fractured porous media: A review of conceptual models and discretization approaches. *Transport in Porous Media*, 130(1):215–236, 2019.
- [10] S. Berrone, S. Pieraccini, and S. Scialò. A PDE-constrained optimization formulation for discrete fracture network flows. *SIAM Journal on Scientific Computing*, 35(2):B487–B510, 2013.
- [11] S. Berrone, S. Pieraccini, and S. Scialò. On simulations of discrete fracture network flows with an optimization-based extended finite element method. *SIAM Journal on Scientific Computing*, 35(2):908–935, 2013.
- [12] S. Berrone, S. Pieraccini, and S. Scialò. An optimization approach for large scale simulations of discrete fracture network flows. *Journal of Computational Physics*, 256(0):838 – 853, 2014.
- [13] S. Berrone, S. Pieraccini, and S. Scialò. Towards effective flow simulations in realistic discrete fracture networks. *Journal of Computational Physics*, 310:181–201, 2016.
- [14] D. Boffi, F. Brezzi, and M. Fortin. *Mixed Finite Element Methods and Applications*. Springer Series in Computational Mathematics. Springer Berlin Heidelberg, 2013.
- [15] W. M. Boon, J. M. Nordbotten, and J. E. Vatne. Functional analysis and exterior calculus on mixed-dimensional geometries. *Annali Matematica Pura ed Applicata*, 2020. In press.
- [16] W. M. Boon, J. M. Nordbotten, and I. Yotov. Robust discretization of flow in fractured porous media. *SIAM Journal on Numerical Analysis*, 56(4):2203–2233, 2018.
- [17] A. Borio, A. Fumagalli, and S. Scialò. Comparison of the response to geometrical complexity of methods for unstationary simulations in discrete fracture networks with conforming, polygonal, and non-matching grids. *Computational Geosciences*, 2020.
- [18] K. Brenner, J. Hennicker, R. Masson, and P. Samier. Gradient discretization of hybrid-dimensional Darcy flow in fractured porous media with discontinuous pressures at matrix-fracture interfaces. *IMA Journal of Numerical Analysis*, Sept. 2016.
- [19] M. Bulíček, J. Málek, and J. Žabenský. A generalization of the Darcy–Forchheimer equation involving an implicit, pressure-dependent relation between the drag force and the velocity. *Journal of Mathematical Analysis and Applications*, 424(1):785–801, 2015.
- [20] C. D’Angelo and A. Scotti. A mixed finite element method for Darcy flow in fractured porous media with non-matching grids. *Mathematical Modelling and Numerical Analysis*, 46(02):465–489, 2012.
- [21] J.-R. de Dreuzy, G. Pichot, B. Poirriez, and J. Erhel. Synthetic benchmark for modeling flow in 3d fractured media. *Computers & Geosciences*, 50:59 – 71, 2013. Benchmark problems, datasets and methodologies for the computational geosciences.

- [22] J. Erhel, J.-R. de Dreuzy, and B. Poirriez. Flow simulation in three-dimensional discrete fracture networks. *SIAM Journal on Scientific Computing*, 31(4):2688–2705, 2009.
- [23] C. Facciola, P. F. Antonietti, and M. Verani. Mixed-primal discontinuous galerkin approximation of flows in fractured porous media on polygonal and polyhedral grids. *PAMM*, 19(1):e201900117, 2019.
- [24] B. Flemisch, I. Berre, W. Boon, A. Fumagalli, N. Schwenck, A. Scotti, I. Stefansson, and A. Tatomir. Benchmarks for single-phase flow in fractured porous media. *Advances in Water Resources*, 111:239–258, January 2018.
- [25] L. Formaggia, A. Fumagalli, A. Scotti, and P. Ruffo. A reduced model for Darcy’s problem in networks of fractures. *ESAIM: Mathematical Modelling and Numerical Analysis*, 48:1089–1116, 7 2014.
- [26] N. Frih, V. Martin, J. E. Roberts, and A. Saâda. Modeling fractures as interfaces with nonmatching grids. *Computational Geosciences*, 16(4):1043–1060, 2012.
- [27] N. Frih, J. E. Roberts, and A. Saada. Modeling fractures as interfaces: a model for Forchheimer fractures. *Computers and Geosciences*, 12(1):91–104, 2008.
- [28] A. Fumagalli and E. Keilegavlen. Dual virtual element method for discrete fractures networks. *SIAM Journal on Scientific Computing*, 40(1):B228–B258, 2018.
- [29] A. Fumagalli and E. Keilegavlen. Dual virtual element methods for discrete fracture matrix models. *Oil & Gas Science and Technology - Revue d’IFP Energies nouvelles*, 74(41):1–17, 2019.
- [30] A. Fumagalli, E. Keilegavlen, and S. Scialò. Conforming, non-conforming and non-matching discretization couplings in discrete fracture network simulations. *Journal of Computational Physics*, 376:694–712, 2019.
- [31] C. Geuzaine and J.-F. Remacle. Gmsh: A 3-d finite element mesh generator with built-in pre- and post-processing facilities. *International Journal for Numerical Methods in Engineering*, 79(11):1309–1331, 2009.
- [32] E. Keilegavlen, R. Berge, A. Fumagalli, M. Starnoni, I. Stefansson, J. Varela, and I. Berre. Porepy: An open-source software for simulation of multiphysics processes in fractured porous media. *Computational Geosciences*, 2020.
- [33] P. Knabner and J. E. Roberts. Mathematical analysis of a discrete fracture model coupling Darcy flow in the matrix with Darcy-Forchheimer flow in the fracture. *ESAIM: Mathematical Modelling and Numerical Analysis*, 48:1451–1472, 9 2014.
- [34] V. Martin, J. Jaffré, and J. E. Roberts. Modeling Fractures and Barriers as Interfaces for Flow in Porous Media. *SIAM Journal on Scientific Computing*, 26(5):1667–1691, 2005.
- [35] F. A. Morales and R. E. Showalter. A Darcy-brinkman model of fractures in porous media. *Journal of Mathematical Analysis and Applications*, 452(2):1332 – 1358, 2017.

- [36] J. M. Nordbotten, W. Boon, A. Fumagalli, and E. Keilegavlen. Unified approach to discretization of flow in fractured porous media. *Computational Geosciences*, 23(2):225–237, 2019.
- [37] P.-A. Raviart and J.-M. Thomas. A mixed finite element method for second order elliptic problems. *Lecture Notes in Mathematics*, 606:292–315, 1977.
- [38] J. E. Roberts and J.-M. Thomas. Mixed and hybrid methods. In *Handbook of numerical analysis, Vol. II*, Handb. Numer. Anal., II, pages 523–639. North-Holland, Amsterdam, 1991.
- [39] I. Rybak and S. Metzger. A dimensionally reduced stokes-Darcy model for fluid flow in fractured porous media. *Applied Mathematics and Computation*, 384:125260, 2020.
- [40] J. J. Salas, H. López, and B. Molina. An analysis of a mixed finite element method for a Darcy–Forchheimer model. *Mathematical and Computer Modelling*, 57(9):2325–2338, 2013. System Dynamics in Project Management & Applied Mathematics and Computational Science and Engineering—Selected Papers of the Seventh PanAmerican Workshop — June 6–11 2010, Venezuela.
- [41] N. Schwenck, B. Flemisch, R. Helmig, and B. Wohlmuth. Dimensionally reduced flow models in fractured porous media: crossings and boundaries. *Computational Geosciences*, 19(6):1219–1230, 2015.
- [42] F. Spena and A. Vacca. A potential formulation of non-linear models of flow through anisotropic porous media. *Transport in Porous Media*, 45:405–421, 12 2001.
- [43] Z. Zeng and R. Grigg. A criterion for non-Darcy flow in porous media. *Transport in Porous Media*, 63(1):57–69, 2006.